Case Rep Dermatol 2011;3:107–112
DOI: 10.1159/000328797

Published online:
May 17, 2011

ISSN 1662–6567
www.karger.com/cde

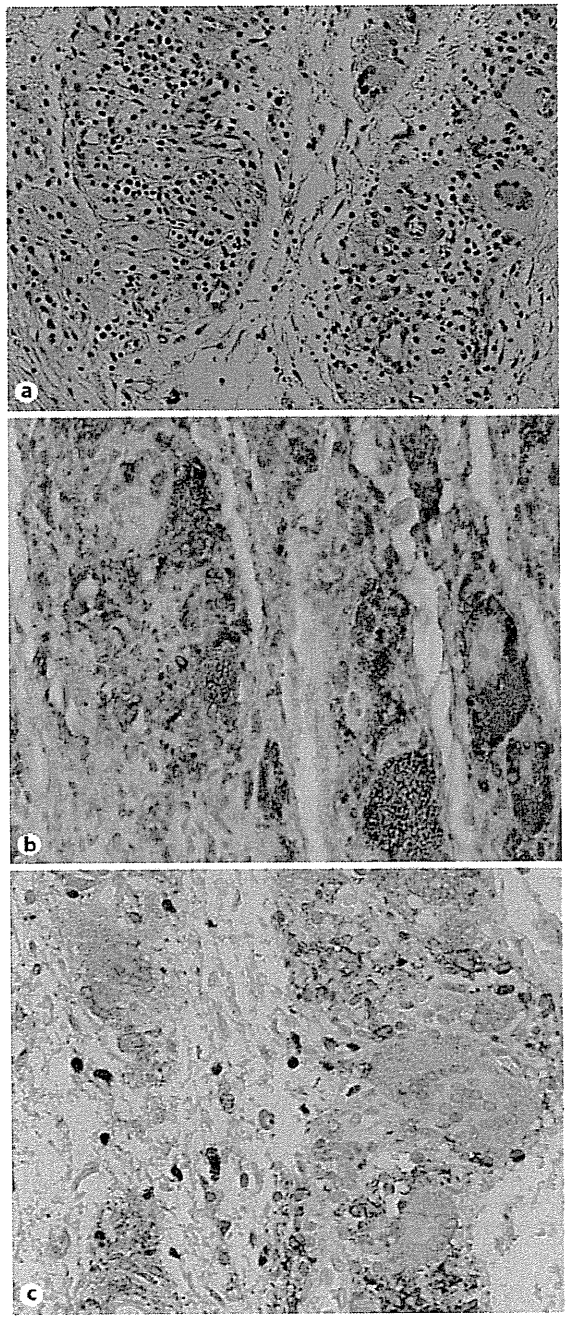

Fig. 2. Histopathological images from hematoxylin-eosin (**a**), original magnification, 100×, and immunohistochemical analyses showing the expression of CD68 (**b**) and CD163 (**c**), original magnification, 200×.

Case Rep Dermatol 2011;3:107–112
DOI: 10.1159/000328797

Published online:
May 17, 2011

ISSN 1662–6567
www.karger.com/cde

References

1 Khamseh ME, Mollanai S, Hashemi F, Rezaizadeh A, Azizi F: Erdheim-Chester syndrome, presenting as hypogonadotropic hypogonadism and diabetes insipidus. J Endocrinol Invest 2002;25:727–729.

2 Tan AP, Tan LK, Choo IH: Erdheim-Chester disease involving breast and muscle: imaging findings. AJR Am J Roentgenol 1995;164:1115–1117.

3 Garg T, Chander R, Gupta T, Mendiratta V, Jain M: Erdheim-Chester disease with cutaneous features in an Indian patient. Skinmed 2008;7:103–106.

4 Pertuiset E, Laredo JD, Liote F, Wassef M, Jagueux M, Kuntz D: [Erdheim-Chester disease: report of a case, review of the literature and discussion of the relation to Langerhans-cell histiocytosis]. Rev Rhum Ed Fr 1993;60:601–609.

5 Veyssier-Belot C, Cacoub P, Caparros-Lefebvre D, Wechsler J, Brun B, Remy M, Wallaert B, Petit H, Grimaldi A, Wechsler B, Godeau P: Erdheim-Chester disease. Clinical and radiologic characteristics of 59 cases. Medicine (Baltimore) 1996;75:157–169.

6 Ginhoux F, Tacke F, Angeli V, Bogunovic M, Loubeau M, Dai XM, Stanley ER, Randolph GJ, Merad M: Langerhans cells arise from monocytes in vivo. Nat Immunol 2006;7:265–273.

7 Brower AC, Worsham GF, Dudley AH: Erdheim-Chester disease: A distinct lipoidosis or part of the spectrum of histiocytosis? Radiology 1984;151:35–38.

8 Waite RJ, Doherty PW, Liepman M, Woda B: Langerhans cell histiocytosis with the radiographic findings of Erdheim-Chester disease. AJR Am J Roentgenol 1988;150:869–871.

9 Kenn W, Eck M, Allolio B, Jakob F, Illg A, Marx A, Mueller-Hermelink HK, Hahn D: Erdheim-Chester disease: Evidence for a disease entity different from Langerhans cell histiocytosis? Three cases with detailed radiological and immunohistochemical analysis. Hum Pathol 2000;31:734–739.

10 Furmanczyk PS, Bruckner JD, Gillespy T 3rd, Rubin BP: An unusual case of Erdheim-Chester disease with features of Langerhans cell histiocytosis. Skeletal Radiol 2007;36:885–889.

11 Schmidt HH, Gregg RE, Shamburek R, Brewer BH Jr, Zech LA: Erdheim-Chester disease: Low low-density lipoprotein levels due to rapid catabolism. Metabolism 1997;46:1215–1219.

12 Murota H, Bae S, Hamasaki Y, Maruyama R, Katayama I: Emedastine difumarate inhibits histamine-induced collagen synthesis in dermal fibroblasts. J Investig Allergol Clin Immunol 2008;18:245–252.

Characterization of dsRNA-induced pancreatitis model reveals the regulatory role of *IFN regulatory factor 2* (*Irf2*) in *trypsinogen5* gene transcription

Hideki Hayashi[a], Tomoko Kohno[a], Kiyoshi Yasui[a], Hiroyuki Murota[b], Tohru Kimura[c], Gordon S. Duncan[d], Tomoki Nakashima[e], Kazuo Yamamoto[d], Ichiro Katayama[b], Yuhua Ma[a], Koon Jiew Chua[a], Takashi Suematsu[a], Isao Shimokawa[f], Shizuo Akira[g], Yoshinao Kubo[a], Tak Wah Mak[d,1], and Toshifumi Matsuyama[a,h,1]

[a]Division of Cytokine Signaling, Department of Molecular Biology and Immunology and [f]Department of Investigative Pathology, Nagasaki University Graduate School of Biomedical Science, Nagasaki 852-8523, Japan; Departments of [b]Dermatology and [c]Pathology, Graduate School of Medicine and [g]Department of Host Defense, Research Institute for Microbial Diseases, Osaka University, Osaka 565-0871, Japan; [d]Campbell Family Cancer Research Institute, Princess Margaret Hospital, Toronto, ON, Canada M5G 2M9; [e]Department of Cell Signaling, Tokyo Medical and Dental University, Tokyo 113-8549, Japan; and [h]Global Center of Excellence Program, Nagasaki University, Nagasaki 852-8523, Japan

Contributed by Tak Wah Mak, October 5, 2011 (sent for review September 8, 2011)

Mice deficient for *interferon regulatory factor* (*Irf*)*2* (*Irf2*$^{-/-}$ mice) exhibit immunological abnormalities and cannot survive lymphocytic choriomeningitis virus infection. The pancreas of these animals is highly inflamed, a phenotype replicated by treatment with poly(I:C), a synthetic double-stranded RNA. Trypsinogen5 mRNA was constitutively up-regulated about 1,000-fold in *Irf2*$^{-/-}$ mice compared with controls as assessed by quantitative RT-PCR. Further knockout of *IFNα/β receptor 1* (*Ifnar1*) abolished poly(I:C)-induced pancreatitis but had no effect on the constitutive up-regulation of *trypsinogen5* gene, indicating crucial type I IFN signaling to elicit the inflammation. Analysis of *Ifnar1*$^{-/-}$ mice confirmed type I IFN-dependent transcriptional activation of dsRNA-sensing pattern recognition receptor genes *MDA5*, *RIG-I*, and *TLR3*, which induced poly(I:C)-dependent cell death in acinar cells in the absence of IRF2. We speculate that Trypsin5, the *trypsinogen5* gene product, leaking from dead acinar cells triggers a chain reaction leading to lethal pancreatitis in *Irf2*$^{-/-}$ mice because it is resistant to a major endogenous trypsin inhibitor, Spink3.

TRIF | IPS-1 | Ca^{2+}-binding proteins | cathepsin B

Interferons (IFNs) are cytokines whose actions contribute to the first line of defense against infection. IFNs both render cells resistant to viral attack and regulate cell growth and differentiation (1). IFNs elicit their pleiotropic effects by regulating the expression of many IFN-stimulated genes (ISGs). IFNs themselves are controlled by IFN regulatory factors (IRFs) that also regulate the expression of ISGs. By binding to IFN-stimulated response elements (ISREs) in gene promoters, the nine known IRF family members (IRF1–9) govern the production of cytokines related to inflammation and immune responses.

When pattern recognition receptors (PRRs) such as Toll-like receptors (TLRs) and retinoic acid-inducible gene-I (RIG)-like receptors detect pathogen ligands, these receptors are activated (2) and transduce downstream signaling, activating IRFs and IFNs. Analyses using knockout (KO) mice deficient for various IRFs have revealed their physiological roles. For example, IRF2 functions mainly as a transcriptional repressor by competing for binding to ISREs with other IRFs, especially IRF9 and IRF1 (1).

Irf2-deficient (*Irf2*$^{-/-}$) mice spontaneously develop inflammatory skin disease as they age, and die within weeks from lymphocytic choriomeningitis virus (LCMV) infection (3). Ablation of *IFNα/β receptor 1* (*Ifnar1*) or *Irf9* ameliorates the skin inflammation of *Irf2*$^{-/-}$ mice, suggesting that IRF2 negatively regulates gene expression by antagonizing IRF9, which is activated by type I IFN (I-IFN) (4). However, the precise mechanisms underlying the phenotypes of *Irf2*$^{-/-}$ are not known. In this study, we found that poly(I:C) (pIC) mimicked LCMV-induced pancreatitis, and we have used double KO mice to explore the cause of death in pIC-treated *Irf2*$^{-/-}$ mice. Our results show that significant trypsinogen5 up-regulation in *Irf2*$^{-/-}$ mice together with I-IFN-dependent transcriptional activation of dsRNA-sensing PRRs were critical for the pIC-induced death.

Results and Discussion

***Irf2*$^{-/-}$ Mice Show IFN-Dependent Poly(I:C)-Induced Pancreatitis and IFN-Independent Secretory Dysfunction in Pancreatic Acinar Cells.** LCMV-infected *Irf2*$^{-/-}$ mice die within 4 wk postinfection (3), but all *Irf2*$^{-/-}$ mice challenged intraperitoneally with poly(I:C) (pIC-*Irf2*$^{-/-}$ mice) died within 1 wk (Fig. 1*A*). Severe acute pancreatitis was apparent in pIC-*Irf2*$^{-/-}$ mice, as shown by abundant TUNEL^{+} apoptotic cells (Fig. 1*B*). Even in the absence of pIC, however, some abnormalities were detected in *Irf2*$^{-/-}$ pancreas, as indicated by hematoxylin and eosin staining (Fig. 1*C*) and electron microscopy (Fig. 1*D*). A mild infiltration of inflammatory cells (particularly lymphocytes) was noted around *Irf2*$^{-/-}$ ductal cells, but this pancreatitis was not typical. The pancreatic acinar cells in untreated *Irf2*$^{-/-}$ mice were filled with eosinophilic secretory granules of heterogeneous size, whereas fewer eosinophilic granules of more uniform size were observed mainly in the apical region of WT acinar cells. Interestingly, treatment of *Irf2*$^{-/-}$ mice with the stable cholecystokinin (CCK) analog cerulein (5) did not cause acute pancreatitis, as assessed by electron microscopy and serum amylase levels (Fig. S1 *A* and *B*). Because mRNA expression of CCK receptors in *Irf2*$^{-/-}$ mice was normal (Fig. S1*C*), these results suggest that the secretory and/or vesicle transport systems in *Irf2*$^{-/-}$ mice are dysfunctional.

The mRNAs encoding the Ca^{2+}-binding proteins Anxa10, Ahsg, and S100-G involved in Ca^{2+}-dependent vesicle transport, sorting, and fusion processes were significantly up-regulated in *Irf2*$^{-/-}$ pancreas (Table S1). The secretory dysfunction observed in cerulein-treated *Irf2*$^{-/-}$ mice (6), which is due to an abnormal distribution pattern of normal levels of soluble *N*-ethylmaleimide-sensitive factor attachment protein receptors (SNAREs) (6), may be due to the abnormal expression of these Ca^{2+}-binding proteins in the absence of IRF2, because annexin family proteins are known to bind and regulate SNAREs (7).

Skin inflammation in *Irf2*$^{-/-}$ mice was rescued by abolishing IFN signaling (4). We asked whether the atypical pancreatitis in *Irf2*$^{-/-}$ mice could be similarly rescued by crossing the *Irf2*$^{-/-}$ mutants to *Ifnar1*-, *Irf1*-, or *Trif*-deficient mice (3, 8, 9) to gen-

Author contributions: H.H., T. Kohno, I.K., T.W.M., and T.M. designed research; H.H., T. Kohno, K. Yasui, H.M., T. Kimura, G.S.D., T.N., K. Yamamoto, Y.M., K.J.C., T.S., and T.M. performed research; T. Kimura, I.S., and S.A. contributed new reagents/analytic tools; Y.K. and T.W.M. analyzed data; and H.H. and T.M. wrote the paper.

The authors declare no conflict of interest.

Freely available online through the PNAS open access option.

[1]To whom correspondence may be addressed. E-mail: tmak@uhnres.utoronto.ca or tosim@nagasaki-u.ac.jp.

This article contains supporting information online at www.pnas.org/lookup/suppl/doi:10.1073/pnas.1116273108/-/DCSupplemental.

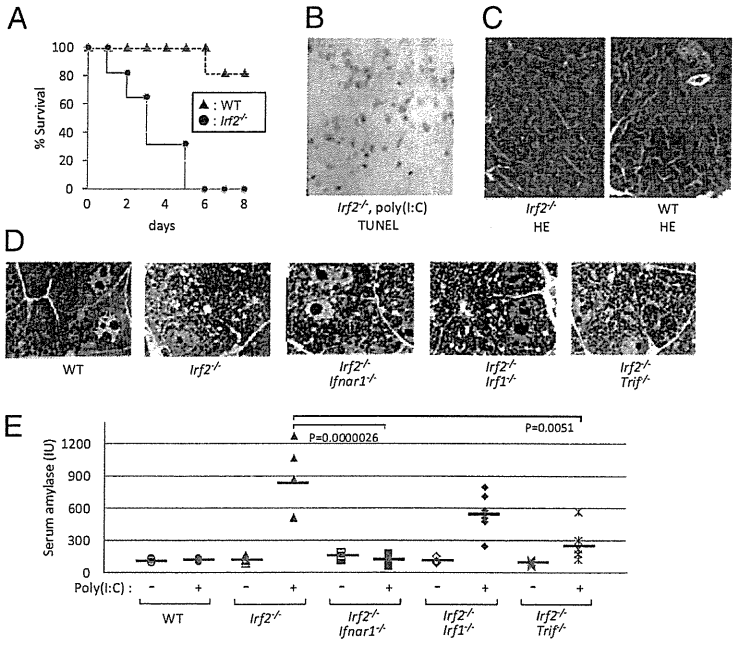

Fig. 1. *Irf2* deficiency induces sensitivity to poly(I:C) and pancreatitis. (*A*) Survival curve after pIC challenge. WT and *Irf2*-deficient ($Irf2^{-/-}$) mice were induced by i.p. pIC challenge (250 μg). All of the $Irf2^{-/-}$ mice were deceased within a week, compared with WT mice. (*B*) Following pIC stimulation, many cells were TUNEL-positive, indicating apoptosis and severe acute pancreatitis in $Irf2^{-/-}$ mice. (*C* and *D*) Hematoxylin and eosin (HE) staining (*C*) and electron microscopic observation (*D*) were done to examine the pancreas histologically in WT, $Irf2^{-/-}$, and double KO mice ($Irf2^{-/-}Ifnar1^{-/-}$, $Irf2^{-/-}Irf1^{-/-}$, and $Irf2^{-/-}Trif^{-/-}$). (*E*) To assess pancreatitis, we monitored serum amylase levels with (+) and without (–) pIC challenge.

erate double knockout mice. Abnormal acinar granule distribution was again observed in $Irf2^{-/-}Ifnar1^{-/-}$, $Irf2^{-/-}Irf1^{-/-}$, and $Irf2^{-/-}Trif^{-/-}$ mice (Fig. 1*D*). Thus, the abnormal acinar structure caused by *Irf2* disruption is not mediated by IFN signaling.

To assess pancreatitis in double knockout mice, we measured serum amylase levels before and after pIC challenge (Fig. 1*E*). Serum amylase was elevated in pIC-$Irf2^{-/-}$ and pIC-$Irf2^{-/-}Irf1^{-/-}$ mice. However, this increase did not occur at all in pIC-$Irf2^{-/-}Ifnar1^{-/-}$ mice, and only to a limited extent in pIC-IRF2$^{-/-}$TRIF$^{-/-}$ mice. These data indicate that type I IFN signaling via IFNAR1, as well as TLR signaling via the adaptor protein TRIF, are important for the development of pIC-induced pancreatitis in $Irf2^{-/-}$ mice. Moreover, our results show that IRF2 regulates IFN-independent pathways affecting acinar cell secretion as well as IFN-dependent pathways inducing pIC-mediated pancreatitis.

Up-Regulated Trypsinogen5 mRNA in the Pancreas of $Irf2^{-/-}$ Mice. We used an Affymetrix DNA microarray system to compare mRNA expression in the pancreas before and after pIC injection of $Irf2^{-/-}$ and WT mice (Fig. 2*A*). In $Irf2^{-/-}$ mice, 14 annotated genes were up-regulated and 8 genes were down-regulated more than 10-fold (Table S1) compared with WT mice. The transcriptional profiles of genes important for the etiology of pancreatitis (10, 11) are listed in Table 1. Strikingly, trypsinogen5 mRNA was up-regulated >100-fold in pIC-$Irf2^{-/-}$ pancreas, a noteworthy observation because trypsinogens activate many other pancreatic enzymes, and premature intracellular activation of trypsinogens in pancreatic acinar cells triggers acute pancreatitis (10, 11). There are 20 *trypsinogen* genes (*T1–T20*) in the murine T-cell receptor β gene locus (12), 12 of which express trypsinogen proteins (Fig. S2, *Right*), whereas humans have only 3 *trypsinogen* genes encoding three proteins: PRSS1, PRSS2, and PRSS3 (Fig. S2, *Left*) (13). The gene expression profile of pIC-$Irf2^{-/-}$ pancreas is inflammation-prone: Mouse trypsinogen mRNAs of T11 (Prss3) and T4 (Trypsinogen5) were up-regulated (Table 1); the mRNA encoding cysteine protease cathepsin B (Ctsb), an enzyme that can initiate pancreatitis by activating trypsinogens (14–16), was also up-regulated (Table 1). The mRNA encoding chymotrypsin C (Ctrc) was down-regulated and another anti-inflammatory factor inter-α-trypsin inhibitor was also down-regulated, although the mRNA encoding Kazal type 3 (Spink3), a serine protease inhibitor that blocks trypsin activity (17), was slightly up-regulated.

We examined the tissue specificity and dependency on IRF2 and IFNAR1 of trypsinogen5 expression by quantitative RT-PCR. In untreated WT mice, trypsinogen5 is expressed most highly in pancreas and skin and modestly in spleen (Fig. S3*A*). In untreated $Irf2^{-/-}$ mice, trypsinogen5 expression in the pancreas was up-regulated ~1,000-fold compared with controls, and was not affected by IFNAR1 ablation. Trypsinogen5 mRNA was up-regulated in $Irf2^{-/-}$ spleen to a much lower extent than in $Irf2^{-/-}$ pancreas, and was not detectable in liver or lung of WT or $Irf2^{-/-}$ mice.

We examined the effects of various IRFs on the activity of the murine *trypsinogen5* promoter, which contains seven ISREs. We cloned a 1.1-kb fragment of the *trypsinogen5* promoter region (–1063 to +15) to create a series of promoter deletion construct mutants driving the firefly luciferase reporter gene (Fig. 2*B*, *Left*). These were transfected into HEK293T cells along with plasmids overexpressing murine IRF1, human IRF5, IRF7, or MyD88. MyD88 was required for IRF-mediated activation of *trypsinogen5* ISREs, and significant promoter activity was observed when IRF1, IRF5, or IRF7 was overexpressed (Fig. S3*B*). Furthermore, the –216 to +15 promoter region of *trypsinogen5* was sufficient for responses to IRF1 or IRF7 stimulation (Fig. S3*C*). Overexpression of IRF2 inhibited IRF1- or IRF7-stimulated promoter activity in a dose-dependent manner (Fig. S3*D*). These data suggest that IRF2 binds to the proximal promoter of *trypsinogen5* and inhibits the access of IRF1, IRF5, and IRF7 to ISRE sites in this region.

To confirm this hypothesis, we transfected TGP49 cells, a mouse acinar cell line, with *trypsinogen5* promoter deletion series reporters as well as with plasmids expressing IRF1, -5, or -7, and assessed the promoter activities (Fig. 2*B*, *Right*). The basal promoter activity was drastically decreased by deleting the –216 to –100 region containing two ISREs, a nuclear factor-activated T cell (NFAT), and an activator protein 1 (AP-1) binding site. In contrast to 293T cells, the *trypsinogen5* promoter in TGP49 cells could be activated by exogenously expressed IRF5 or IRF7 without MyD88 (Fig. 3*A*). The promoter could not be activated by IRF1 even in the presence of MyD88 expression. The regions responsive to IRF5 and IRF7 were confirmed to be ISRE4 (–62 to –59) and ISRE3 (–55 to –49) by site-specific mutation analysis (Fig. 2*C*). The IRF5- and IRF7-dependent promoter activities were significantly ($P < 0.05$) enhanced by knocking down Irf2 with specific siRNA compared with control (scrambled) siRNA (Fig. 3*A*).

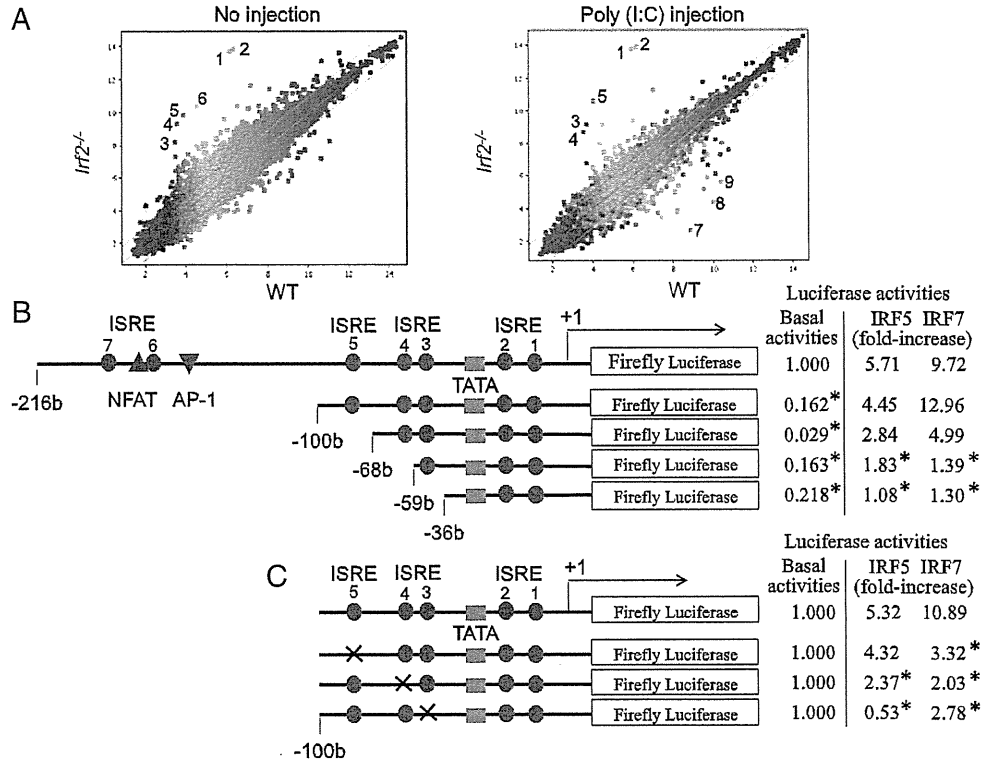

Fig. 2. Trypsinogen5 is highly expressed in *Irf2*-deficent mice. (*A*) *Irf2*$^{-/-}$ or wild-type mice with or without peritoneal injection of pIC were killed, and the amounts of mRNA from the pancreas were systematically compared using Affymetrix 28,815 gene probes. The points farthest from the diagonal indicate transcripts showing the greatest difference between WT and *Irf2*$^{-/-}$. Points 1 and 2, trypsinogen5 with different probes; 3, α-2-HS-glycoprotein (Ahsg); 4, annexin A10 (Anxa10); 5, fetuin-β (Fetub); 6, 3-hydroxy-3-methylglutaryl-CoenzymeA synthase2 (Hmgcs2, HMG-CoA synthase); 7, Ig κ chain variable8 (Igk-V8); 8, unknown; 9, carbonic anhydrase 3 (Car3). (*B*) A series of deletion mutants of *trypsinogen5* proximal promoter region (−216 to +15) was placed upstream of a luciferase reporter gene (1 μg) and analyzed for transcriptional activity in mouse pancreatic acinar cells using a dual luciferase assay at 24 h posttransfection in combination with expression vectors (100 ng) expressing IRF5 or IRF7 or a control vector. The basal luciferase activity of each deletion, measured relative to the −216 to +15 region, and the responses to IRF5 and IRF7 expression vectors are shown as fold increase compared with the control vector. The TATA box, ISRE core, and NFAT- and AP-1 binding sites are indicated. *$P < 0.05$ versus the −216 to +15 region. (*C*) Point mutations were introduced into each ISRE site (indicated by x) of the *trypsinogen5* promoters as described in *Materials and Methods*. The promoter activity of each mutant *trypsinogen5* was determined with a dual luciferase assay system. *$P < 0.05$ versus wild type.

To confirm IRF2 binding to the proximal promoter of trypsinogen5 in pancreatic acinar cells in vivo, we performed chromatin immunoprecipitation (ChIP) assays in TGP49 cells using specific PCR probes spanning all seven ISREs (−173 to +56) in the *trypsinogen5* promoter. Anti-IRF2 antibody specifically precipitated the *trypsinogen5* promoter, as determined by semiquantitative PCR (Fig. 3*B*) and real-time PCR (Fig. 3*C*). These results suggest that in WT mice, trypsinogen5 expression in pancreatic acinar cells is repressed by the binding of IRF2 to ISREs in the proximal promoter region. However, in *Irf2*$^{-/-}$ mice, the *trypsinogen5* gene is activated because IRF5 and IRF7 can access the ISREs in the absence of IRF2.

IRF5 and IRF7 are critical inducers of the expression of proinflammatory cytokines and type I IFNs, respectively (18, 19), and these activities require MyD88. In WT cells, IRF4 inhibits IRF5 function by sequestering MyD88 (18). IRF2 did not associate with MyD88 (18) but, in our study, it did bind to the ISRE-containing region in the trypsinogen5 promoter (Fig. 3 *B* and *C*). Therefore, we postulate that IRF2 inhibits IRF5 and IRF7 activity by competing with them for binding to ISREs, rather than by sequestering MyD88.

Trypsinogen5 Is Resistant to the Trypsin Inhibitor Spink3. Comparison of mouse trypsinogen5 to other mouse and human trypsinogens (Fig. S4) showed that, although the N-terminal activation peptide sequence (NSDDK-I) in trypsinogen5 differs from that in other trypsinogens (DDDDK-I), other important regions, including the triad amino acid sequence H-D-S, required for enzymatic activity are conserved (10, 11). In addition, tryptic activity in cell lysates of 293FT cells overexpressing trypsinogen5 was dramatically enhanced by treatment with enteropeptidase (Fig. 4 *A* and *B*). The trypsinogen5 inhibitor binding site (DSCDGDS), which prevents premature activation, differed from that found in most trypsinogens (DSCQGDS) (10, 11), resembling the inhibitor binding site (DSCQRDS) of the human trypsin inhibitor-resistant PRSS3 enzyme. In addition, the trypsin autolytic cleavage site (Q-V) in trypsinogen5 differed from that in other trypsinogens (R-V), suggesting that trypsinogen5 is resistant to both trypsin inhibitors and self-inactivation. Indeed, trypsinogen5 was resistant to inhibition by Spink3, a major en-

Table 1. Expressions of relevant genes to pancreatitis

Gene transcripts	WT (−)	WT (pIC)	*Irf2*$^{-/-}$ (−)	*Irf2*$^{-/-}$ (pIC)
Prss1 (T16, Trypsin1)	11,161	13,863	10,388	13,788
Prss2 (T20, Trypsin 2)	16,041	15,661	15,857	15,494
Prss3 (T11, Trypsin 3)	1,155	1,131	3,059 ↑	2,395 ↑
Trypsinogen5 (T4, 1810009J06Rik)	70	57	13,514 ↑	14,287 ↑
Chymotrypsin C (Ctrc)	545	368	87 ↓	119 ↓
Chymotrypsinogen B 1 (Ctrb1)	19,417	18,772	20,457	19,919
Amylase2-2, pancreatic (Amy2b)	19,101	18,488	17,092	18,261
Calcium-sensing receptor (Casr)	37	37	30	26
Cystic fibrosis membrane conductance regulator (Cftr)	7	6	11	8
Cathepsin B (Ctsb)	349	443	848 ↑	794 ↑
Serine protease inhibitor, Kazal-type 3 (Spink3)	4,716	3,957	7,497	7,774
Inter-α-trypsin inhibitor, heavy chain 4 (Itih4)	375	212	78 ↓	71 ↓
Galanin (Gal)	879	1,057	213 ↓	71 ↓

The levels of gene expression in the pancreas are shown in Affymetrix units. The trypsinogen5 data are Point 1 in Fig. 2.

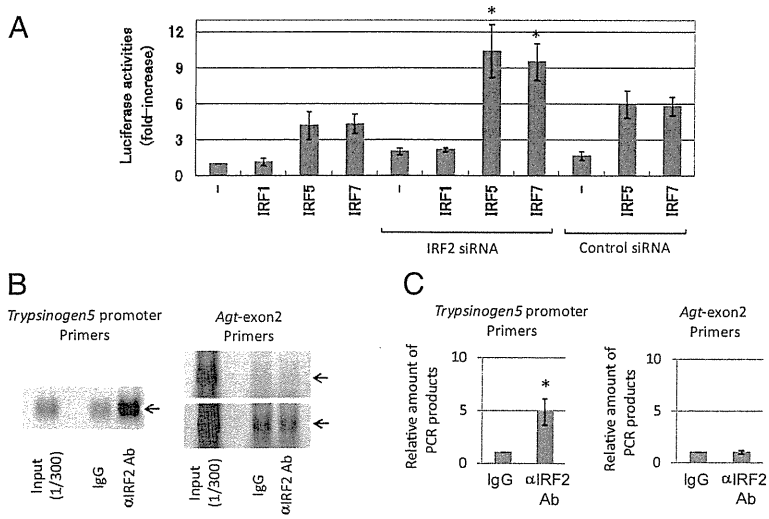

Fig. 3. IRF2 binds to the promoter region of *trypsinogen5* gene. (*A*) The effects of siRNAs (3 μg) specific to IRF2 or a control scrambled sequence on transcriptional activity of the −216 to +15 luciferase reporter in TGP49 acinar cells were measured. $*P < 0.05$ versus control siRNA. (*B*) A chromatin immunoprecipitation assay was done using TGP49 acinar cells with the IRF2-specific antibody (5 μg) or the same amount of control nonspecific IgG. The precipitated chromatin fragments were detected by PCR with a *trypsinogen5* promoter-specific primer set at 35 cycles or a negative control primer set for *angiotensinogen* (*Agt*) exon2 at 30 (*Upper*) and 35 (*Lower*) cycles. The input before precipitation indicates the predicted size (Trp5, 229 bp; Agt, 221 bp) of the PCR product. (*C*) The ChIP assay done in *B* was quantitatively measured using a real-time PCR method with the same primers. The relative amounts of β-actin were calculated, and the amounts of chromatin fragments precipitated with the anti-IRF2 antibody were shown relative to those with the nonspecific control antibody (IgG). $*P < 0.01$ versus control IgG.

dogenous trypsin inhibitor in mice (Fig. 4 *C* and *D*), as well as by soy bean trypsin inhibitor (Fig. S5 *A* and *B*). Analysis of the evolutionary pedigree in Fig. S6 showed that mouse trypsinogen5 is most distant from mPrss1 and mPrss2, just as human PRSS3 is most distant from PRSS1 and PRSS2. Therefore, we believe that mouse trypsinogen5 is a homolog of human PRSS3. Moreover, our data suggest that, in the absence of IRF2, trypsinogen5 is highly expressed and exacerbates pIC-induced pancreatitis due to its inhibitor-resistant nature.

Poly(I:C)-Induced Cell Death Can Be Triggered by a TLR3/TRIF-Dependent Pathway or a RIG-I/MDA5/IPS-1-Dependent Pathway. Although trypsinogen5 was up-regulated in untreated IRF2$^{-/-}$ mice, only mild inflammation around acinar cells was observed and pancreatitis did not occur. We hypothesize that trypsinogen5 as well as mPrss1, -2, and -3 leaking from dying acinar cells are activated by proteases such as cathepsin B or enteropeptidase, also released from these cells. These activated trypsins trigger signals to induce the death of many acinar cells, a process of cell death amplification we refer to as the "enhancing loop" of acinar cell death. In this way, the initial death of a few cells induced by pIC can precipitate severe pancreatitis. This idea is supported by a report that the extracellular or intracellular treatment of pancreatic acinar cells with active trypsins causes acinar cell death (20). In this study, the enteropeptidase cleavage site (-DDDDK-) of rat trypsinogen was replaced with a cleavage site (-RTKR-) recognized by paired basic amino acid-cleaving enzyme (PACE). This allowed the rat trypsinogen to be activated intracellularly with the ubiquitously expressed PACE enzyme rather than with enteropeptidase, which is expressed mainly in the duodenum. We created a PACE-trypsinogen5 enzyme that successfully induced the apoptosis of 293FT cells when overexpressed (Fig. 4 *E* and *F*). These results indicate that proteolytic activation of trypsinogen5 is sufficient to induce cell death.

Because pIC-dependent pancreatitis in *Irf2*$^{-/-}$ mice can be prevented by inactivating IFNAR1 signaling (Fig. 1*E*), we focused on IFN signaling pathways to identify candidates that might trigger initial cell death following pIC treatment. Indeed,

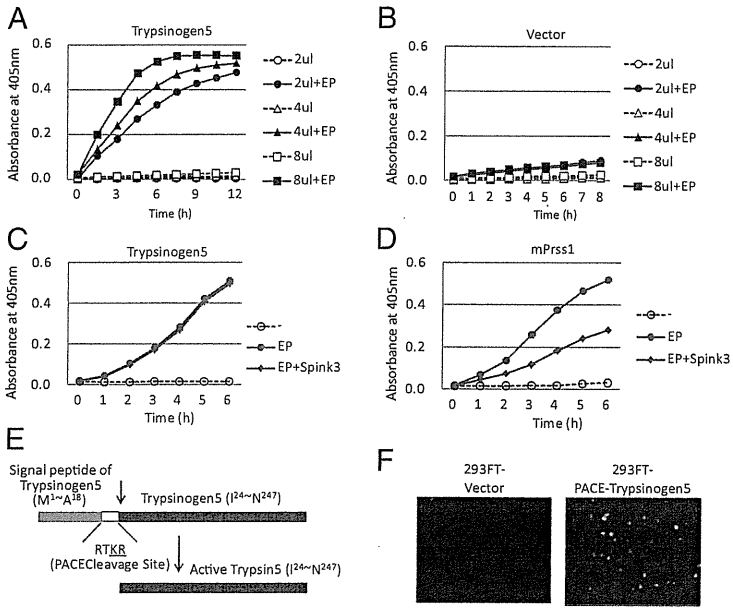

Fig. 4. Trypsinogen activity is activated by proteolytic cleavage. (*A* and *B*) A full-length mouse trypsinogen5 cDNA from the mouse pancreas was cloned into pcDNA3 (Invitrogen) and expressed in 293T cells. The indicated amounts of cell lysates (2–8 μL of 5 μg/μL lysates) were mixed with a trypsin-specific substrate (BioVision) in the presence or absence of added enteropeptidase. Tryptic activity was monitored by the amount of released pNA, measuring spectrophotometric units (A_{405}). (*C* and *D*) The effects of Spink3 were examined by adding cell lysates expressing Spink3, a major intrinsic trypsin inhibitor in mouse pancreas, to lysates expressing trypsinogen5 (*C*) or mouse Prss1 (*D*). (*E*) The DNA sequence encoding the activation peptide in the trypsinogen5 expression vector was replaced with sequences encoding a PACE cleavage site (-RTKR-) so that tryptic activity is activated by ubiquitously expressed PACE protease. (*F*) 293FT cells transfected with PACE-trypsinogen5 or control vector were stained with FITC-labeled annexin V to detect apoptosis.

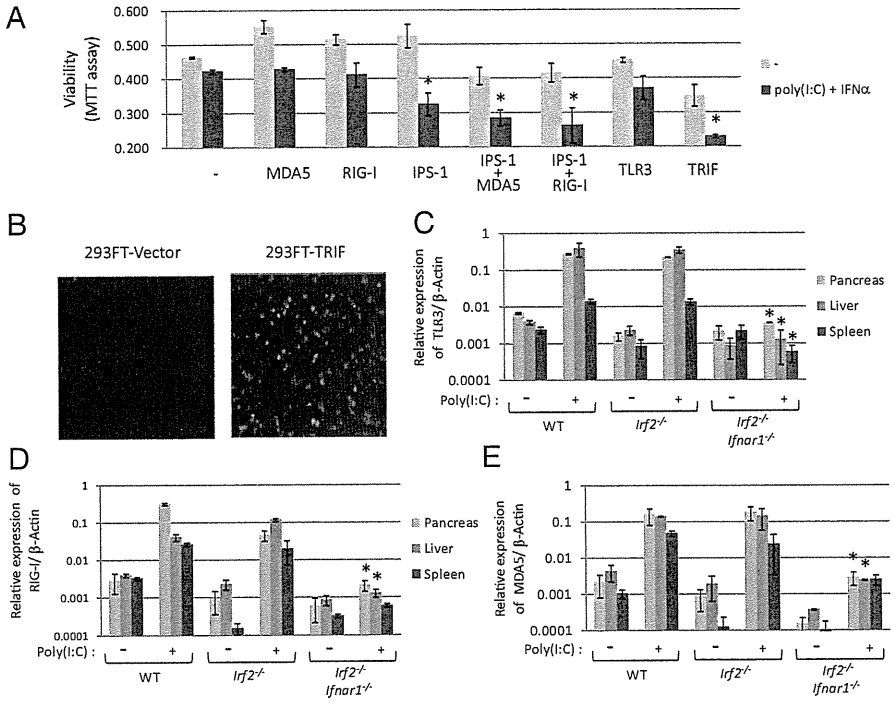

Fig. 5. Poly(I:C) and IFNα treatment induces cell death through different pathways. (*A*) Viabilities of 293FT cells transfected with the indicated expression plasmids in the presence or absence of pIC (5 μg/mL) and IFNα (50 ng/mL) for 44 h were quantified with the MTT assay. The values represent the average of at least three separate experiments, with SDs shown by error bars. TRIF and IPS-1 with MDA5 or RIG-I induced significant ($*P < 0.02$) cell death in response to pIC and IFNα. (*B*) 293FT cells transfected with TRIF expression vector or vector alone were stained with FITC-labeled annexin V to detect apoptosis. mRNA expression levels of TLR3 (*C*), RIG-I (*D*), and MDA5 (*E*) were measured using real-time PCR with (+) or without (–) i.p. pIC injection (250 μg). mRNAs prepared from pancreas, liver, and spleen of WT, *Irf2*$^{-/-}$, and *Irf2*$^{-/-}$*Ifnar1*$^{-/-}$ mice were converted into cDNA, and the amount of cDNA was determined by real-time PCR with the specific primers listed in *SI Materials and Methods*. The values represent the average of at least two mice, with SDs shown by error bars. $*P < 0.05$ versus *Irf2*$^{-/-}$ mice.

IRF1, *IRF7*, *MyD88*, *MDA5*, *RIG-I*, and *TLR3* gene expression were all up-regulated in the pancreas of pIC-*Irf2*$^{-/-}$ mice (Table S2). Because these proteins are associated with cell death pathways dependent on TRIF or IPS-1, we examined the effect of IRF2 loss on these well-characterized systems (21, 22). TRIF binds to receptor-interacting proteins and thereby activates caspase8 via FADD to induce cell death (21), whereas the IPS-1-dependent cell death pathway, which is triggered by MDA5 or RIG-I, is reported to activate caspase9 via the mitochondrial pathway dependent on Apaf-1 and cytochrome *c* (22). We confirmed that 293FT cells transfected with TRIF-expressing plasmid underwent apoptosis, as shown by staining with FITC-labeled annexin V (Fig. 5*B*). Next, we used the MTT viability assay to quantify the extent of cell death induced by IFN-related molecules in the presence or absence of pIC and IFNα. Exogenous overexpression of IPS-1 or TRIF significantly enhanced the death of pIC- and IFN-treated 293FT cells, and the death-inducing effects of MDA5 and RIG-I were enhanced by cotransfection with IPS-1 (Fig. 5*A*). These results suggest the existence of at least two pIC-dependent cell death pathways: one TLR3/TRIF-dependent and one RIG-I/MDA5/IPS-1-dependent.

We used real-time PCR to examine the induction of TLR3, RIG-I, and MDA5 mRNAs in pIC-treated WT, *Irf2*$^{-/-}$, and *Irf2*$^{-/-}$*Ifnar1*$^{-/-}$ mice. The levels of all three mRNAs were induced by nearly 100-fold in both pIC-WT and pIC-*Irf2*$^{-/-}$ mice, and these increases were abolished by deletion of IFNAR1 (Fig. 5 *C–E*). The IFN signal activation triggered by pIC is essential to initiate TLR3/TRIF- and RIG-I/MDA5/IPS-1-dependent acinar cell death, but is not sufficient to cause pancreatitis (Table S3). The elevation of trypsinogen5 expression mediated by abolishing IRF2 is also necessary for enhancing the cell death leading to lethal pancreatitis.

Activation Mechanisms of Mouse Trypsinogen5 and Human PRSS3. Trypsinogens (including trypsinogen5) can be activated in pancreatic acinar cells, or in other cells or tissues by enteropeptidase expressed in nonduodenal cells (23) such as in keratinocytes and oral carcinoma cells (24, 25). It is possible that keratinocyte-expressed enteropeptidase activates the trypsinogen5 expressed in skin (Fig. S3*A*), promoting age-dependent skin inflammation in *Irf2*$^{-/-}$ mice (4). Another possibility could be that proteases in addition to enteropeptidase can cleave pancreatic trypsinogen5. We have confirmed that cathepsin B, whose expression was elevated in *Irf2*$^{-/-}$ mice, can activate trypsinogen5 in vitro (Fig. S5*C*). The last possibility is that autocatalytic cleavage of trypsinogen, usually restricted under steady-state conditions, is accelerated in response to chemical stress or viral infection. Indeed, the autoactivation of trypsinogen is reportedly accelerated in low pH or by Ca^{2+} in vitro (26).

In conclusion, this study has identified important genes associated with IRF2 functions in mice. Our results suggest that IRF2 influences the expression of mouse trypsinogen5, whose human counterpart is PRSS3. Our data should therefore help to elucidate new IRF functions in humans.

Materials and Methods

Mice. *Irf1*$^{-/-}$ and *Irf2*$^{-/-}$ mice have been described (3). *IFNα/β receptor 1* (*Ifnar1*)$^{-/-}$ mice were purchased from B&K Universal (8). TRIF$^{-/-}$ mice have been described (9). *Irf2*$^{-/-}$*Ifnar1*$^{-/-}$, *Irf2*$^{-/-}$*Irf1*$^{-/-}$, and *Irf2*$^{-/-}$*Trif*$^{-/-}$ double mutant mice were generated by crossing *Irf2*$^{+/-}$ with *Ifnar1*$^{-/-}$, *Irf1*$^{-/-}$, and *Trif*$^{-/-}$ mice, respectively. All mice were maintained under specific pathogen-free conditions and used at 6–12 wk of age. All experiments were performed according to institutional guidelines.

Cells. Human embryonic kidney (HEK)293T and 293FT (Invitrogen) cells and HeLa cells were cultured in DMEM supplemented with 10% FBS. Mouse pancreatic acinar TGP49 cells were cultured in a 1:1 mixture of DMEM and Ham's F-12 medium supplemented with 10% FBS.

Histological Analysis. Pancreas tissues were fixed overnight in 10% formalin, embedded in paraffin, sectioned, and stained with hematoxylin (0.4%) and eosin (0.5%) for light microscopic analysis. For electron microscopic analysis, the tissues were fixed in 2.5% glutaraldehyde solution buffered to pH 7.4 with 0.1 M phosphate buffer for 4 h at 4 °C. Postfixation was performed with 2% osmium tetroxide solution buffered to pH 7.4 with the same buffer for 2 h at 4 °C, and they were embedded, sectioned, and doubly stained with uranyl acetate and lead nitrate.

Microarrays. Total RNAs from the pancreas of wild-type and *Irf2*$^{-/-}$ mice aged 6 wk, harvested 3 h after no injection or a peritoneal injection with 250 μg poly(I:C), were used in the array studies. The quality of the RNA was assessed with an Agilent 2100 Bioanalyzer, and samples of 100 ng total RNA were reverse-transcribed and then amplified by in vitro transcription according to Affymetrix standard protocols. The mouse Affymetrix GeneChip Mouse Gene 1.0 ST Array was used in all hybridizations. These arrays contain probes representing transcripts for 28,815 mouse gene entities. Microarray data were analyzed using Affymetrix Expression Console software and Gene Spring GX, whereas differentially expressed genes were identified with annotation.

Real-Time RT-PCR. Total RNA was prepared from tissues using the acid phenol-guanidinium thiocyanate method after immersing the tissues for more than overnight in RNAlater Solution (Ambion). Reverse transcription was conducted for 60 min at 46 °C from 200 ng of purified total RNA using SuperScript III (Invitrogen), followed by 45 cycles of PCR (15-s denaturation at 95 °C, 25-s annealing at 55 °C, and 15-s extension at 72 °C). An SYBR Green PCR Kit (Qiagen) was used to monitor the PCR products on a LightCycler 1.5 and real-time PCR detection system (Roche). Primers designed for the respective genes are listed in *SI Materials and Methods*.

Plasmid Constructs. cDNAs encoding human IRF5, IRF7, and IPS-1 were generated from total RNA prepared from 293T cells by RT-PCR using KOD-FX DNA polymerase (Toyobo). Human MDA5, RIG-I, and TLR3 cDNAs were generated from total RNA prepared from THP-1 (a human leukemia cell line) or HeLa cells by RT-PCR. Mouse Trypsinogen5, Prss1, and Spink3 cDNAs were made from total RNA prepared from WT mouse pancreas by PCR. All constructs generated by PCR were confirmed by DNA sequencing. The p*Trypsinogen5*-Luc reporter plasmid was constructed by inserting the promoter region (−1063 to +15) of the mouse *trypsinogen5* gene by PCR into the pGL2-Basic vector. A series of deletion mutants was prepared using proper restriction enzymes (NcoI at −833; SpeI at −579; ScaI at −386; PvuII at −216) and a specific primer for the −100 site. The promoter region (−216 to +15) of the mouse *trypsinogen5* gene was used to introduce point mutations into the ISREs. The point mutations of ISRE3 (−55 to −49, ATTGAAA→GTTTGCG), ISRE4 (−62 to −59, TTTC→CGCA), and ISRE5 (−84 to −78, AATGAAA→GATTGCG) were introduced by overlap PCR mutagenesis. All constructs generated by PCR were confirmed by DNA sequencing.

PACE-Trypsinogen5 was constructed by replacing the activation peptide (-NSDDK-) of mouse trypsinogen5 cDNA with the PACE recognition peptide (-RTKR-) by overlap PCR mutagenesis.

Luciferase Reporter Assay. 293T cells (1 × 10^5 per well) were plated in 24-well plates and transfected 24 h later with 200 ng of the firefly luciferase reporter plasmid p*Trypsinogen5*-Luc, using FuGENE6 (Roche), along with each expression vector (20 ng unless otherwise stated) as indicated. In all cases, cells were transfected with 20 ng pRL-TK (*thymidine kinase* promoter-driven Renilla luciferase reporter gene; Promega) to normalize the transfection efficiency. TGP49 cells (1 × 10^5 per well) were plated in 12-well plates and transfected 24 h later with 1 μg of the firefly luciferase reporter plasmid pTrypsinogen5-Luc using Lipofectamine 2000 (Invitrogen), along with each expression vector (100 ng unless otherwise stated) as indicated. In all cases, cells were transfected with 20 ng pRL-RSV (RSV promoter-driven Renilla luciferase reporter gene). At 26 h posttransfection, luciferase activity was determined with a dual luciferase assay system (Promega). Mouse IRF2-specific and control siRNAs were purchased from Santa Cruz Biotechnology.

Chromatin Immunoprecipitation. Nuclear extracts from TGP49 cells were subjected to DNA–protein cross-linking with 1% formaldehyde for 5 min. After extensive washing, the samples were suspended in 500 μL of 150 mM NaCl, 25 mM Tris (pH 7.5), 5 mM EDTA, 1% Triton X-100, 0.1% SDS, and 0.5% deoxycholate and sonicated. After centrifugation at 14,000 rpm for 10 min at 4 °C, the supernatants were immunoprecipitated with 0.5 μg anti-IRF2 antibody, or the corresponding IgG (Sigma) (as a control), and Protein A Sepharose4B Fast Flow beads. The amounts of precipitated DNA were quantified by PCR using a pair of mouse *Trypsinogen5* promoter-specific primers and *Angiotensinogen* exon2-specific primers (*SI Materials and Methods*).

Trypsin Activity Assay. Trypsin activity was monitored by the amount of released *p*-nitroanilide (pNA) from a specific substrate, measuring spectrophotometric units at 405 nm (A_{405}) (Trypsin Activity Assay Kit; BioVision). Cell lysates prepared at 48 h posttransfection of the indicated expression plasmids were used with or without enteropeptidase (light chain, porcine; GenScript).

Cell Death Assay. Pancreatic tissues were used in a TUNEL assay. Briefly, tissue sections were incubated with 20 μg/mL proteinase K for 20 min, followed by inhibition of endogenous peroxidase by incubation with 2% H_2O_2 for 7 min. TdT (GIBCO-BRL) and biotinylated dUTP (Roche) in TdT buffer [0.1 M potassium cacodylate (pH 7.2), 2 mM $CoCl_2$, 0.2 mM DTT] were added to the sections and incubated in a humid atmosphere at 37 °C for 90 min after immersion in TdT buffer. The reaction was terminated by transferring the slides to TB buffer (300 mM NaCl, 30 mM Na citrate) for 30 min. The sections were covered with 10% rabbit serum for 10 min and then with the avidin–biotin peroxidase complex for 30 min. Finally, 3,3′-diaminobenzidine (DAB) was used as the chromogen. To detect apoptotic cells, FITC-conjugated annexin V (BioVision) was used according to the manufacturer's instruction. An MTT (ICN) assay to assess living cells was performed according to the manufacturer's instruction.

ACKNOWLEDGMENTS. This work was supported by Grants-in-Aid from the Ministry of Education, Culture, Sports, Science and Technology of Japan (22659092) and by the Global Center of Excellence Program at Nagasaki University.

1. Savitsky D, Tamura T, Yanai H, Taniguchi T (2010) Regulation of immunity and oncogenesis by the IRF transcription factor family. *Cancer Immunol Immunother* 59:489–510.
2. Kawai T, Akira S (2011) Toll-like receptors and their crosstalk with other innate receptors in infection and immunity. *Immunity* 34:637–650.
3. Matsuyama T, et al. (1993) Targeted disruption of IRF-1 or IRF-2 results in abnormal type I IFN gene induction and aberrant lymphocyte development. *Cell* 75:83–97.
4. Hida S, et al. (2000) CD8(+) T cell-mediated skin disease in mice lacking IRF-2, the transcriptional attenuator of interferon-α/β signaling. *Immunity* 13:643–655.
5. Lampel M, Kern H-F (1977) Acute interstitial pancreatitis in the rat induced by excessive doses of a pancreatic secretagogue. *Virchows Arch A Pathol Anat Histol* 373:97–117.
6. Mashima H, et al. (2011) Interferon regulatory factor-2 regulates exocytosis mechanisms mediated by SNAREs in pancreatic acinar cells. *Gastroenterology* 141:1102–1113.
7. Gerke V, Creutz C-E, Moss S-E (2005) Annexins: Linking Ca^{2+} signalling to membrane dynamics. *Nat Rev Mol Cell Biol* 6:449–461.
8. Hwang SY, et al. (1995) A null mutation in the gene encoding a type I interferon receptor component eliminates antiproliferative and antiviral responses to interferons α and β and alters macrophage responses. *Proc Natl Acad Sci USA* 92:11284–11288.
9. Yamamoto M, et al. (2003) Role of adaptor TRIF in the MyD88-independent Toll-like receptor signaling pathway. *Science* 301:640–643.
10. Chen J-M, Férec C (2009) Chronic pancreatitis: Genetics and pathogenesis. *Annu Rev Genomics Hum Genet* 10:63–87.
11. Whitcomb D-C (2010) Genetic aspects of pancreatitis. *Annu Rev Med* 61:413–424.
12. Spicuglia S, Pekowska A, Zacarias-Cabeza J, Ferrier P (2010) Epigenetic control of Tcrb gene rearrangement. *Semin Immunol* 22:330–336.
13. Rowen L, et al. (2005) Interchromosomal segmental duplications explain the unusual structure of PRSS3, the gene for an inhibitor-resistant trypsinogen. *Mol Biol Evol* 22:1712–1720.
14. Figarella C, Miszczuk-Jamska B, Barrett A-J (1988) Possible lysosomal activation of pancreatic zymogens. Activation of both human trypsinogens by cathepsin B and spontaneous acid. Activation of human trypsinogen 1. *Biol Chem Hoppe Seyler* 369 (Suppl):293–298.
15. Halangk W, et al. (2000) Role of cathepsin B in intracellular trypsinogen activation and the onset of acute pancreatitis. *J Clin Invest* 106:773–781.
16. Meister T, et al. (2010) Missorting of cathepsin B into the secretory compartment of CI-MPR/IGFII-deficient mice does not induce spontaneous trypsinogen activation but leads to enhanced trypsin activity during experimental pancreatitis—without affecting disease severity. *J Physiol Pharmacol* 61:565–575.
17. Hashimoto D, et al. (2008) Involvement of autophagy in trypsinogen activation within the pancreatic acinar cells. *J Cell Biol* 181:1065–1072.
18. Negishi H, et al. (2005) Negative regulation of Toll-like-receptor signaling by IRF-4. *Proc Natl Acad Sci USA* 102:15989–15994.
19. Honda K, et al. (2005) Spatiotemporal regulation of MyD88-IRF-7 signalling for robust type-I interferon induction. *Nature* 434:1035–1040.
20. Ji B, Gaiser S, Chen X, Ernst S-A, Logsdon C-D (2009) Intracellular trypsin induces pancreatic acinar cell death but not NF-&kappaB activation. *J Biol Chem* 284: 17488–17498.
21. Kaiser W-J, Offermann M-K (2005) Apoptosis induced by the Toll-like receptor adaptor TRIF is dependent on its receptor interacting protein homotypic interaction motif. *J Immunol* 174:4942–4952.
22. Lei Y, et al. (2009) MAVS-mediated apoptosis and its inhibition by viral proteins. *PLoS One* 4:e5466.
23. Yahagi N, et al. (1996) Complementary DNA cloning and sequencing of rat enteropeptidase and tissue distribution of its mRNA. *Biochem Biophys Res Commun* 219:806–812.
24. Nakanishi J, Yamamoto M, Koyama J, Sato J, Hibino T (2010) Keratinocytes synthesize enteropeptidase and multiple forms of trypsinogen during terminal differentiation. *J Invest Dermatol* 130:944–952.
25. Vilen S-T, et al. (2008) Intracellular co-localization of trypsin-2 and matrix metalloprotease-9: Possible proteolytic cascade of trypsin-2, MMP-9 and enterokinase in carcinoma. *Exp Cell Res* 314:914–926.
26. Chen J-M, et al. (2003) Evolution of trypsinogen activation peptides. *Mol Biol Evol* 20: 1767–1777.

11β-Hydroxysteroid Dehydrogenase-1 Is a Novel Regulator of Skin Homeostasis and a Candidate Target for Promoting Tissue Repair

Mika Terao[1*¤], Hiroyuki Murota[1], Akihiro Kimura[1], Arisa Kato[1], Akiko Ishikawa[1], Ken Igawa[1], Eiji Miyoshi[2], Ichiro Katayama[1]

1 Department of Dermatology, Graduate School of Medicine, Osaka University, Suita, Osaka, Japan, **2** Department of Molecular Biochemistry and Clinical Investigation, Osaka University, Suita, Osaka, Japan

Abstract

11β-hydroxysteroid dehydrogenase 1 (11β-HSD1) catalyzes the interconversion of cortisone and cortisol within the endoplasmic reticulum. 11β-HSD1 is expressed widely, most notably in the liver, adipose tissue, and central nervous system. It has been studied intensely over the last 10 years because its activity is reported to be increased in visceral adipose tissue of obese people. Epidermal keratinocytes and dermal fibroblasts also express 11β-HSD1. However, the function of the enzymatic activity 11β-HSD1 in skin is not known. We found that 11β-HSD1 was expressed in human and murine epidermis, and this expression increased as keratinocytes differentiate. The expression of 11β-HSD1 by normal human epidermal keratinocytes (NHEKs) was increased by starvation or calcium-induced differentiation *in vitro*. A selective inhibitor of 11β-HSD1 promoted proliferation of NHEKs and normal human dermal fibroblasts, but did not alter the differentiation of NHEKs. Topical application of selective 11β-HSD1 inhibitor to the dorsal skin of hairless mice caused proliferation of keratinocytes. Taken together, these data suggest that 11β-HSD1 is involved in tissue remodeling of the skin. This hypothesis was further supported by the observation that topical application of the selective 11β-HSD1 inhibitor enhanced cutaneous wound healing in C57BL/6 mice and *ob/ob* mice. Collectively, we conclude that 11β-HSD1 is negatively regulating the proliferation of keratinocytes and fibroblasts, and cutaneous wound healing. Hence, 11β-HSD1 might maintain skin homeostasis by regulating the proliferation of keratinocytes and dermal fibroblasts. Thus 11β-HSD1 is a novel candidate target for the design of skin disease treatments.

Citation: Terao M, Murota H, Kimura A, Kato A, Ishikawa A, et al. (2011) 11β-Hydroxysteroid Dehydrogenase-1 Is a Novel Regulator of Skin Homeostasis and a Candidate Target for Promoting Tissue Repair. PLoS ONE 6(9): e25039. doi:10.1371/journal.pone.0025039

Editor: Marian Ludgate, Cardiff University, United Kingdom

Received March 29, 2011; **Accepted** August 26, 2011; **Published** September 20, 2011

Funding: This work was supported in part by a Grant-in-Aid for Scientific Research(C) No. 21591464 from the Japan Society for the Promotion of Science. The funders had no role in study design, data collection and analysis, decision to publish, or preparation of the manuscript. No additional external funding received for this study.

Competing Interests: The authors have declared that no competing interests exist.

* E-mail: mterao@derma.med.osaka-u.ac.jp

¤ Current address: Department of Dermatology, Graduate School of Medicine, Osaka University, Suita, Osaka, Japan

Introduction

The endogenous steroid hormone glucocorticoid (GC) is released in response to various stressors such as physical injury and psychological stress. It regulates biological processes including growth, development, metabolism, and behavior [1,2]. In mammalian cells, it induces diverse responses including differentiation, proliferation, and apoptosis [3].

GC is the most effective anti-inflammatory drug for treating acute and chronic inflammatory diseases, and has been used for more than half a century. The major anti-inflammatory mechanism of GC is the repression of inflammatory gene transcription factors such as nuclear factor κB and activator protein-1 [1,4]. Topical application of GC ointment is one of the most common treatments for inflammatory dermatitis, and its mechanism is thought to be its anti-inflammatory effects on keratinocytes and skin infiltrating inflammatory cells. In addition to its strong anti-inflammatory effects, GC also influences keratinocyte biology in other ways. Microarray analyses have revealed that dexamethasone, a synthetic glucocorticoid, regulates genes associated with differentiation, metabolism, and inflammation in keratinocytes [5].

Cortisol is the endogenous GC in humans. The enzyme 11β-hydroxysteroid dehydrogenase (11β-HSD) is known to catalyze the interconversion between hormonally active cortisol and inactive cortisone in cells [6,7,8]. The two iso-enzymes of 11β-HSD both reside in the endoplasmic reticulum membrane [9]. The 11β-HSD1 isoform, which catalyzes the conversion of cortisone to cortisol, is widely expressed at the highest levels in the liver, lung, adipose tissue, ovary, and central nervous system. The 11β-HSD2 isoform, which catalyzes the conversion of cortisol to cortisone, is highly expressed in the distal nephron, colon, sweat glands, and placenta. Because 11β-HSD1 activity is reported to be elevated in the visceral adipose tissue of obese people, it has been studied intensely over the last 10 years [10,11,12]. Targeted overexpression of 11β-HSD1 in adipose tissue in mice has been found to model metabolic syndrome [13,14].

Recently, 11β-HSD1 was found to be expressed in epidermal keratinocytes, dermal fibroblasts, and outer hair follicle root sheath

cells. 11β-HSD1 expression increases with age in primary dermal fibroblasts and in skin tissues [15,16]. Furthermore, Cirillo et al. demonstrated enzymatic activity of 11β-HSDs in keratinocyte in culture [17]. While these results suggested that 11β-HSDs have functions in skin component cells, the *in vivo* functions of 11β-HSDs, in skin homeostasis remained unclear.

In this study, we demonstrate that 11β-HSD1 is critical for skin homeostasis, which functions by modulating keratinocyte and fibroblast proliferation. In addition, we show the effect of topical application of a selective inhibitor of 11β-HSD1 on mouse skin and cutaneous wound healing, which collectively may demonstrate the possibility of 11β-HSD1 as a novel target in treating cutaneous disease.

Materials and Methods

Cell culture

Normal human epidermal keratinocytes (NHEKs) and normal human dermal fibroblasts (NHDFs) were purchased from DS Pharma Biomedical (Osaka, Japan). NHEKs were cultured on type-1 collagen-coated plates (Asahi Techno Glass, Funabashi, Japan) in human keratinocyte serum-free medium (DS Pharma Biomedical) supplemented with bovine pituitary extract. Dulbecco's modified Eagle's medium (DMEM) containing 10% fetal bovine serum (FBS) was used to culture NHDFs. Isolation and culture of mouse keratinocytes and mouse fibroblasts were carried out as previously described [18]. Full-thickness skin harvested from day 2 to day 4 newborn mice was treated with 4 mg/ml of dispase (Gibco; Invitrogen, Paisley, UK) for 1 h at 37°C. Next, the epidermis was peeled from the dermis. The epidermis was trypsinized to prepare single cells. It was then incubated in Human Keratinocyte Serum Free Medium for 6 h at 37°C under an atmosphere with 5% CO_2. Non-adherent cells were washed away with phosphate-buffered saline (PBS) twice, and then cultured for 2–3 days in human keratinocyte serum free medium before use in experiments. The dermis was placed in PBS+0.05% type-1 collagenase (Sigma-Aldrich, St Louis, MO, USA) and incubated at 37°C for 30 min with vigorous agitation to prepare single cells. After filtration, cells were centrifuged at 200 g for 10 min, resuspended in DMEM+10% FBS, and incubated at 37°C and in 5% CO_2. First or second passage fibroblasts were used for experiments.

Histopathological analysis

Samples of normal skin from healthy volunteers were taken after written informed consent. All studies were approved by the ethical committee of Osaka University. Samples were fixed in 10% formaldehyde for 24 h, followed by embedding in paraffin and microtome sectioning. Slides were stained with hematoxylin and eosin (H&E). For immunohistochemical analysis, sections were hydrated by passage through xylene and graded ethanols. After antigen retrieval for 10 min at 90°C in citric buffer, pH 6.0, the slides were blocked with serum-free protein block (Dako-Cytomation, Carpinteria, CA, USA) for 10 min, then incubated with primary antibody overnight at 4°C (rabbit anti-11β-HSD1 antibody 1:100 dilution, Abcam, Cambridge, UK; rabbit anti-Ki-67 antibody 1:500 dilution, Novocastra Laboratories Ltd, Newcastle, UK). After washing with tris-buffered saline (TBS) containing 0.05% Triton-X100, slides were mounted using the Vectastain ABC kit® (Vector Laboratories, Burlingame, CA, USA) followed by counterstaining with haematoxylin. Rabbit IgG were used as the isotype controls. For immunofluorescent analysis, sections were hydrated as described above and incubated with primary antibody (rabbit anti-11β-HSD1 antibody 1:100 dilution and mouse anti-keratin 14 antibody 1:500 dilution, Abcam), followed by secondary antibody (anti-rabbit Alexa Fluor 555 and anti-mouse Alexa Fluor 488, Invitrogen).

Western blotting

Cell samples were solubilized at 4°C in lysis buffer (0.5% sodium deoxycholate, 1% Nonidet P40, 0.1% sodium dodecyl sulphate, 100 μg/ml phenylmethylsulphonyl fluoride, 1 mM sodium orthovanadate, and protease inhibitor cocktail). For *in vivo* samples, skins were crushed in liquid nitrogen and solubilized at 4°C in lysis buffer. Ten micrograms of protein were separated on SDS-polyacrylamide gels and transferred onto polyvinylidine fluoride membranes (Bio-Rad, Hercules, CA, USA). Non-specific protein binding was blocked by incubating the membranes in 5% w/v non-fat milk powder in TBS-T (50 mM Tris-HCl, pH 7.6, 150 mM NaCl, and 0.1% v/v Tween-20). The membranes were incubated with sheep anti-11β-HSD1 antibody (The Binding Site, Birmingham, UK), rabbit anti-keratin 1 antibody (Covance, Emeryville, CA, USA), and anti-involucrin (IVL) antibody (Santa Cruz Biotechnology, Santa Cruz, CA, USA) at a dilution of 1:1000 overnight at 4°C or with mouse monoclonal anti-β-actin (Sigma-Aldrich, St. Louis, MO, USA) at a dilution of 1:5000 for 30 min at room temperature. Then, the membranes were washed three times in TBS-T for 5 min. Finally, the membranes were incubated with either HRP-conjugated anti-rabbit, anti-mouse, or anti-sheep antibody at a dilution of 1:10,000 for 60 min at room temperature. Protein bands were detected using the ECL Plus kit (GE Healthcare, Buckinghamshire, UK). The intensity of the bands was quantified by using NIH image J software.

11β-HSD1 inhibitor treatment

11β-HSD1 inhibitor (385581) purchased from Merck (Whitehouse Station, NJ, USA) is a potent inhibitor of 11β-HSD1 with >450- and >100-fold selectivity over human and mouse 11β-HSD2, respectively [19]. The inhibitor was dissolved in DMSO and further diluted more than 100,000-fold in culture medium (for *in vitro* experiments), in a 1:1 mixture of acetone:olive oil (for *in vivo* topical application), or in PBS (for *in vivo* wound healing). DMSO was used as a vehicle control.

MTS cell viability assay

Cellular viability was assessed using CellTiter96® Aqueous One Solution Cell Proliferation Assay (Promega, Madison, WI, USA). Briefly, NHEKs or NHDFs were seeded onto 96-well plates (5000 cells/well or 500 cells/well in 100 μl medium, respectively). The cells were allowed to attach for 24 h and then incubated with 11β-HSD1 inhibitor or vehicle control at the indicated doses for 48 h. Next, 20 μl of MTS reagent was added, and the cells were incubated for 2 h. Optical density was measured at 490 nm with a Micro Plate Reader (Bio-Rad, Hercules, CA, USA).

BrdU incorporation assay

Cell proliferation was assessed using cell proliferation ELISA, BrdU (Roche, Basel, Switzerland) according to the manufacturer's protocol. Briefly, NHEKs were seeded onto 96-well plates (5000 cells/well in 100 μl medium). The cells were allowed to attach for 24 h and then incubated with 11β-HSD1 inhibitor or vehicle control at the indicated doses for 48 h. Next, cells were labeled with BrdU, and incubated for 4 h. BrdU incorporation was quantified by measuring with a Micro Plate Reader (Bio-Rad) at 450 nm.

siRNA transfection

NHEKs (50,000 cells/ml) were seeded on type-1 collagen coated plates 1 day prior to transfection. Cells were transfected with 11β-HSD1 or control siRNAs (Invitrogen) at 50 nM using RNAi MAX (Invitrogen), and the culture medium was replaced 6 h later. Cells were used for experiments 48 h after transfection.

RNA isolation and quantitative real time polymerase chain reaction (rtPCR)

Total RNA was isolated from cells using the SV Total RNA Isolation System (Promega). The product was reverse-transcribed into first-strand complementary DNA (cDNA). Thereafter, the expression of 11β-HSD1, 11β-HSD2, IVL, and keratin 10 (K10) was measured using the Power SYBR Green PCR Master Mix (Applied Biosystems, Foster City, CA) according to the manufacturer's protocol. Glyceraldehyde-3-phosphate dehydrogenase (GAPDH) was used to normalize the mRNA as quantified GAPDH was not affected by the treatment. Similar results were obtained in each experiment when another internal control, β-actin, was used to normalize the mRNA (data not shown). Sequence-specific primers were designed as follows: 11β-HSD1, sense: 5′-tctcctctctggctgggaaag, antisense: 5′- gaacccatccaaagcaaacttg; IVL, sense: 5′-tctgcctcagccttactgtg, antisense: 5′-ggaggaggaacagtcttgagg; K10, sense: 5′-tgaaaagcatggcaactcac, antisense: 5′-tgtcgatctgaagcaggatg; Fibroblast growth factor-2 (FGF-2), sense: 5′-agagcgaccctcacatcaag, antisense: 5′- actgcccagttcgtttcagt; TGF-β, sense: 5′- cacgtggagctgtaccagaa: 5′- gaacccgttgatgtccactt ; Matrix metalloproteinase-1 (MMP-1), sense: 5′- gtgctaaaggtgccaatggt, antisense: 5′- tccttggggtatccgtgtag ; Collagen 1 alpha 1 (Col1a1), sense: 5′- ctcctcgctttccttcctct, antisense: 5′- ctcctcgctttccttcctct ; and GAPDH, sense: 5′- ggagtcaacggatttggtcgta-3′, antisense: 5′- gcaacaatatccactttaccagagttaa-3′. Real-time PCR (40 cycles of denaturation at 92°C for 15 seconds and annealing at 60°C for 60 seconds) was run on an ABI 7000 Prism (Applied Biosystems). Samples without reverse transcriptase (negative control) did not show any amplification.

Cortisol measurement by ELISA

NHEKs (10,000 cells/ml, 100 μl) were seeded on 96-well type-A collagen-coated plates. The cells were allowed to attach for 24 h and then the medium was changed to a high calcium (1.2 mM) basal medium that did not contain bovine pituitary extract, to remove cortisol from the culture media. The culture media were harvested 48 h later. Harvested samples were stored at −20°C until use. The amount of cortisol in samples was measured with an Cortisol EIA kit (Cayman Chemical Company, Ann Arbor, MI, USA).

Wound healing assay

Male C57BL/6 and C57BL/6J-*ob/ob* mice were obtained from Japan Charles River, Inc. Animal care was in accordance with the institutional guidelines of Osaka University. At 6 weeks of age, dorsal hairs were removed by using hair removal cream (epilat, Kracie, Inc., Tokyo, Japan). Full-thickness 15-mm wounds were created on the backs of mice (n = 3 in each group for first experiment and n = 4 in each group for second experiment) a day after hair removal. 11β-HSD1 inhibitor (10 μM) or vehicle control dissolved in PBS was applied to the wound and the wound was covered with hydrocolloid dressing. This application was repeated every 2 days. The wound areas were calculated by measuring the major and minor axes on days, 0, 2, 4, 6, 8, 10, and 12 after wounds were created.

Topical 11β-HSD1 inhibitor treatment

Eight-week-old male Hos: HR-1 mice (hairless mice) were obtained from Japan SLC, Inc. Animal care was in accordance with the institutional guidelines of Osaka University. Mouse dorsal skins (n = 3 in each group for first experiment and n = 5 in each group for second experiment) were treated with 11β-HSD1 inhibitor (50 μM) or vehicle control dissolved in a 1:1 mixture of acetone:olive oil for 5 .continuous days. One day after the last treatment, the treated dorsal skins were harvested for histological analysis.

Statistical analysis

The data are expressed as mean values ± standard deviation (SD). The unpaired Student's *t*-test was used to determine the level of significance of differences between the sample means.

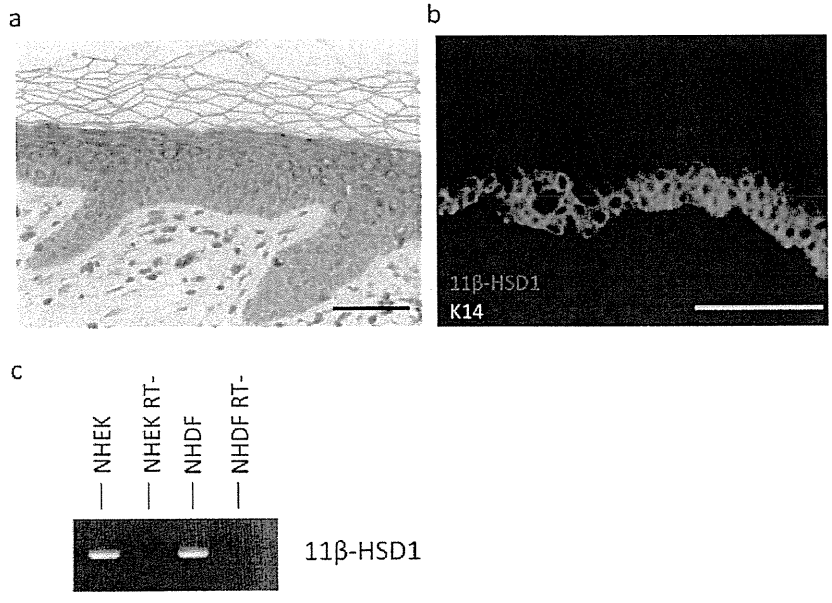

Figure 1. 11β-HSD1 expression in human skin. (a) Immunohistochemical staining of 11β-HSD1 (DAB staining) in normal skin tissue. Bar = 50 μM (b) Immunofluorescent staining of 11β-HSD1 (red) and keratin 14 (green). Bar = 100 μM (c) PCR detecting 11β-HSD1 in NHEKs and NHDFs. RT-: samples without reverse transcriptase (negative control).
doi:10.1371/journal.pone.0025039.g001

Results

11β-HSD1 expression in the skin

First, the expression of 11β-HSD1 in healthy skin was examined. 11β-HSD1 was broadly expressed in all layers of the epidermis and in dermal fibroblasts (Figure 1a). Its expression was stronger in the cytoplasm of supra-basal cells, and only weakly detected in basal cells. This was also confirmed by double staining with both the anti-11β-HSD1 antibody and the basal cell marker, anti-K14 (Figure 1b). The expression of 11β-HSD1 was also detected in cultured NHEKs and in NHDFs (Figure 1c).

11β-HSD1 expression is increased by starvation or calcium induced differentiation

We next investigated whether the starvation and differentiation alter the expression of 11β-HSD1 in NHEKs. Starving keratinocytes by depriving them of pituitary extract in the culture media retards the growth of keratinocytes. Twenty-four hours of starvation significantly increased the expression of 11β-HSD1 (Figure 2a). NHEKs are known to differentiate when 1.2 mM calcium is added. This treatment causes the early differentiation markers keratin 1 (K1), K10, and IVL to increase as the cells differentiate [20,21]. The stimulation of differentiation with 1.2 mM of calcium increased the expression of 11β-HSD1 in NHEKs (Figure 2b and 2c). These results indicate that starvation of essential supplements or calcium-induced differentiation increases the expression of 11β-HSD1 in NHEKs.

11β-HSD1 regulates proliferation, but not differentiation, of NHEKs

To determine if 11β-HSD1 modulated keratinocyte proliferation, we investigated the effect of selective 11β-HSD1 inhibitor on the

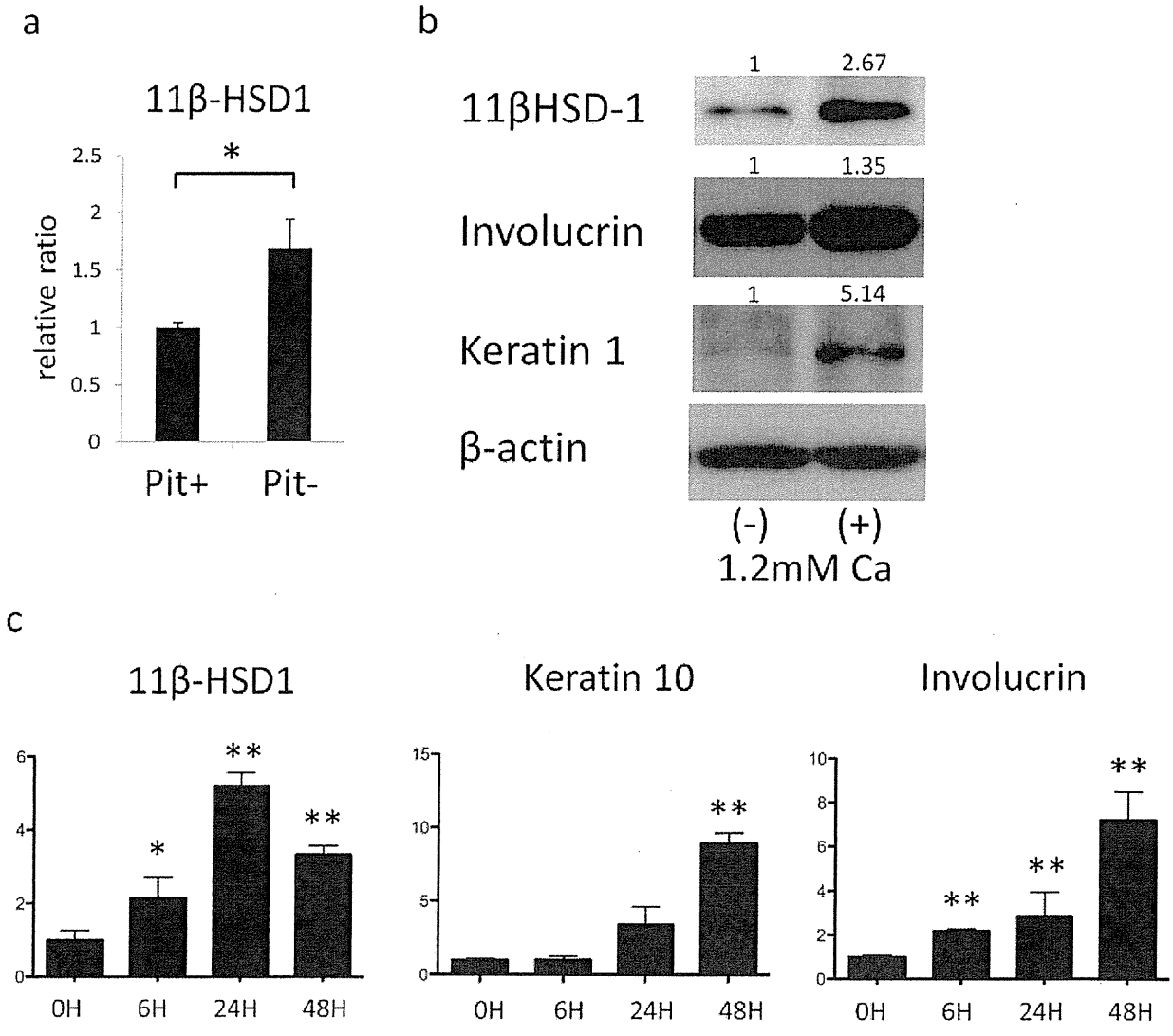

Figure 2. 11β-HSD1 expression is increased with starvation and differentiation. (a) The relative expression of 11β-HSD1 in NHEKs assessed by rtPCR with or without pituitary extract (pit) in culture media. GAPDH was used as an internal control. (b)Western blotting for detecting 11β-HSD1, Keratin 1, and Involucrin 48 h after adding 1.2 mM of calcium to culture media of NHEKs. The numbers indicate the relative ratio to β-actin. (c) The relative expressions of 11β-HSD1, Keratin 10, and Involucrin of the indicated hour after adding 1.2 mM calcium to culture media of NHEKs assessed by rtPCR. GAPDH was used as an internal control. An asterisk indicates a statistically significant difference (*$P<0.05$, **$P<0.01$, Student's *t*-test).
doi:10.1371/journal.pone.0025039.g002

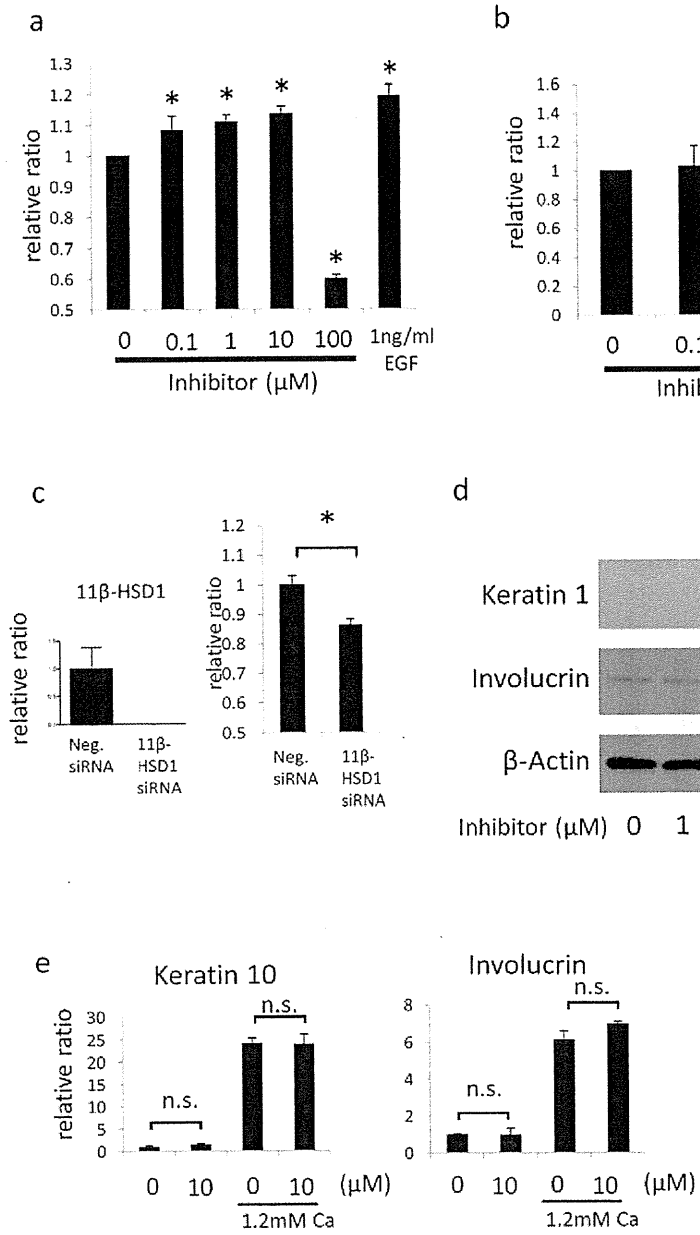

Figure 3. 11β-HSD1 regulates proliferation but not differentiation of NHEKs. (a,b) 11β-HSD1 selective inhibitor was applied to NHEKs at indicated dose and proliferation of the cells was assessed by MTS assay (a) and BrdU absorption (b) 72 h later. DMSO was applied as vehicle control and epidermal growth factor (EGF) was used as positive control in MTS assay. The relative ratio compared with absorbance of vehicle control (0 μM) is suggested. The histograms indicate means and SDs for eight independent experiments. An asterisk (*) indicates a statistically significant difference from the vehicle treated group ($P<0.05$, Student's *t*-test). (c) siRNA knockdown efficacy (left) and MTS assay (right) of NHEKs transfected with 11β-HSD1 or control. Assay was performed 48 h after transfection. Transfection of si11β-HSD1 decreased the mRNA expression 11β-HSD1 more than 95% assessed by rtPCR. GAPDH was used as an internal control. The histograms indicate means and SDs for eight independent experiments. An asterisk (*) indicates a statistically significant difference from the vehicle treated group ($P<0.05$, Student's *t*-test). (d) Western blotting of NHEKs for detecting Keratin 1, and Involucrin treated with 11β-HSD1 selective inhibitor at indicated dose for 72 h with or without 1.2 mM calcium treatment. β-actin was used as an internal control. (e) The relative expressions of Keratin 10 and Involucrin treated with 10 μM 11β-HSD1 selective inhibitor for 48 h with or without 1.2 mM calcium treatment assessed by rtPCR. GAPDH was used as an internal control. n.s.: not significant.
doi:10.1371/journal.pone.0025039.g003

proliferation of NHEKs. Addition of 100 nM–10 μM of inhibitor to culture medium, induced cell proliferation in a dose dependent manner in both MTS assays (Figure 3a) and BrdU absorption assays (Figure 3b), suggesting that 11β-HSD1 inhibits keratinoctye proliferation. In contrast, higher doses (100 μM) of inhibitor decreased cell viability. Knocking down 11β-HSD1 with siRNA also reduced the viability of NHEKs (Figure 3c). These observations suggest that basal levels of 11β-HSD1 are essential for keratinocytes survival, and excessive loss of 11β-HSD1 activity with higher doses of inhibitor (100 μM) or siRNA-mediated depletion, can therefore

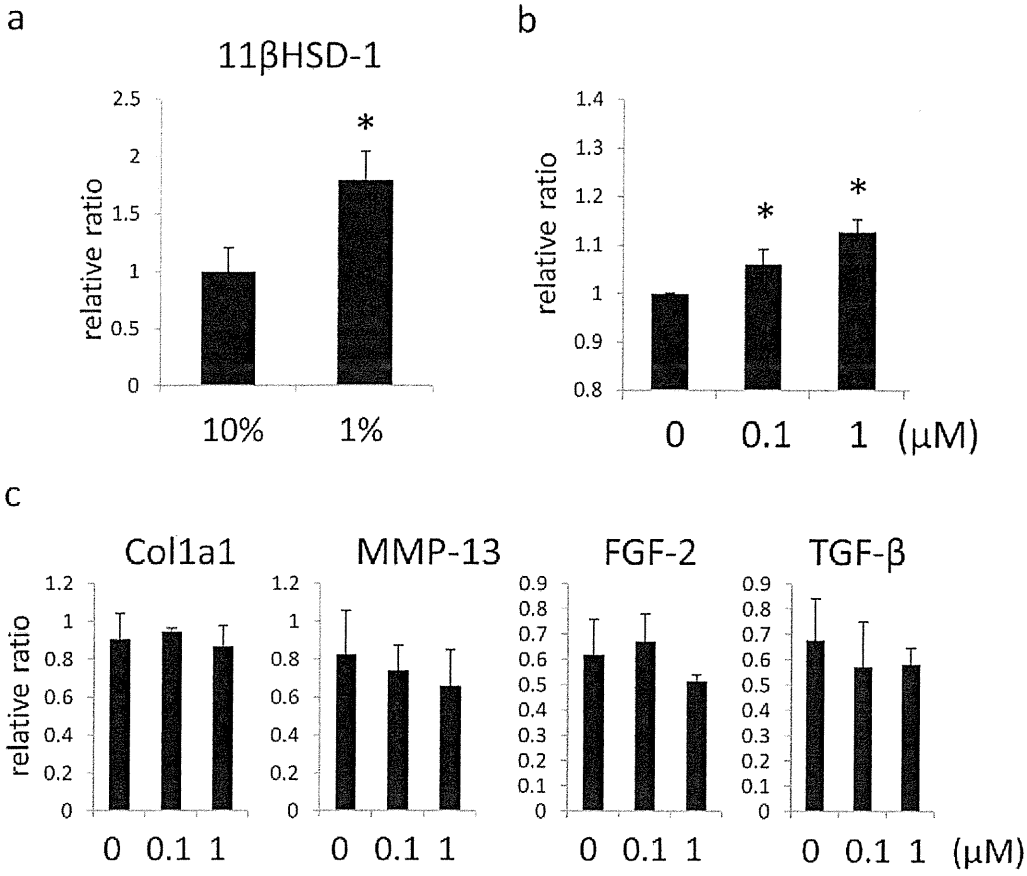

Figure 4. 11β-HSD1 regulates proliferation of NHDFs. (a) The relative expression of 11β-HSD1 in NDHF assessed by rtPCR with 10% FBS or 1% FBS in culture media. GAPDH was used as an internal control. (b) 11β-HSD1 selective inhibitor was applied to NHDFs cultured in DMEM containing 2% FBS at indicated dose and proliferation of the cells was assessed by MTS assay 72 h later. DMSO was applied as vehicle control. The histograms indicate means and SDs for eight independent experiments. An asterisk (*) indicates a statistically significant difference from the vehicle treated group ($P<0.05$, Student's *t*-test). (c) The relative expressions of Col1a1, MMP-1, FGF-2, TGF-β treated with 11β-HSD1 selective inhibitor at indicated dose for 48 h assessed by rtPCR. GAPDH was used as an internal control.
doi:10.1371/journal.pone.0025039.g004

not be used to evaluate the functions of 11β-HSD1 in cortisol production, proliferation, or differentiation of keratinocytes.

Next, we evaluated the effects of 11β-HSD1 inhibitor on the calcium-stimulated differentiation of NHEKs. Although calcium treatment increased the expression of 11β-HSD1, protein and mRNA for K1 or K10, and IVL were not affected by 1 to 10 μM of selective 11β-HSD1 inhibitor (Figure 3d,e). These results indicated that 11β-HSD1 might be involved in the proliferation but not in the differentiation of NHEKs.

11β-HSD1 regulates proliferation of NHDFs

We next investigated the function of 11β-HSD1 in NHDFs. Starving NHDFs by reducing medium concentrations of FBS from 10% to 1% for 24 h retards cell growth. The expression of 11β-HSD1 was significantly enhanced in starvation conditions (Figure 4a). Furthermore, similarly to the effects on keratinocytes, the selective 11β-HSD1 inhibitor at doses of 100 nM and 1 μM induced proliferation of NHDFs, demonstrating that 11β-HSD1 also negatively regulates NHDFs proliferation (Figure 4b). Next, the effect of 11β-HSD1 inhibitor on the expression of fibrogenic cytokines and fibroblast growth factors was evaluated (Figure 4c). However, inhibition of 11β-HSD1 at these doses did not affect the expression of Col1a1, MMP-13, TGF-β, or FGF-2. This indicates that 11β-HSD1 was not involved in collagen metabolism, and inhibits the proliferation of NHDFs via pathways independent of the autocrine effects of these cytokines and growth factors.

Topical application of 11β-HSD1 inhibitor induces hyperproliferation of the epidermis

To investigate the function of 11β-HSD1 *in vivo*, hairless mouse skin was exposed to 11β-HSD1 inhibitor.. 11β-HSD1 is also expressed in the epidermis and fibroblasts of murine skin in C57BL/6 mice and Hos: HR-1 (hairless) mice (Figure 5a,b,d,e). The expression of 11β-HSD1 was also detected in cultured primary mouse keratinocytes and in cultured primary dermal fibroblasts derived from C57BL/6 and Hos: HR-1 mice (Figure 5c,f). Application of 50 μM selective 11β-HSD1 inhibitor to the dorsal skin of Hos: HR-1 mice for five continuous days induced acanthosis (Figure 5g). The epidermal thickness was significantly higher in selective 11β-HSD1 inhibitor treated groups than control groups (Figure 5h). In addition, the number of Ki-67 positive cells was significantly higher in 11β-HSD1 inhibitor treated skin than in vehicle treated skin (Figure 5i,j). These results demonstrate that 11β-HSD1 inhibitor also promotes the proliferation of keratinocytes *in vivo*.

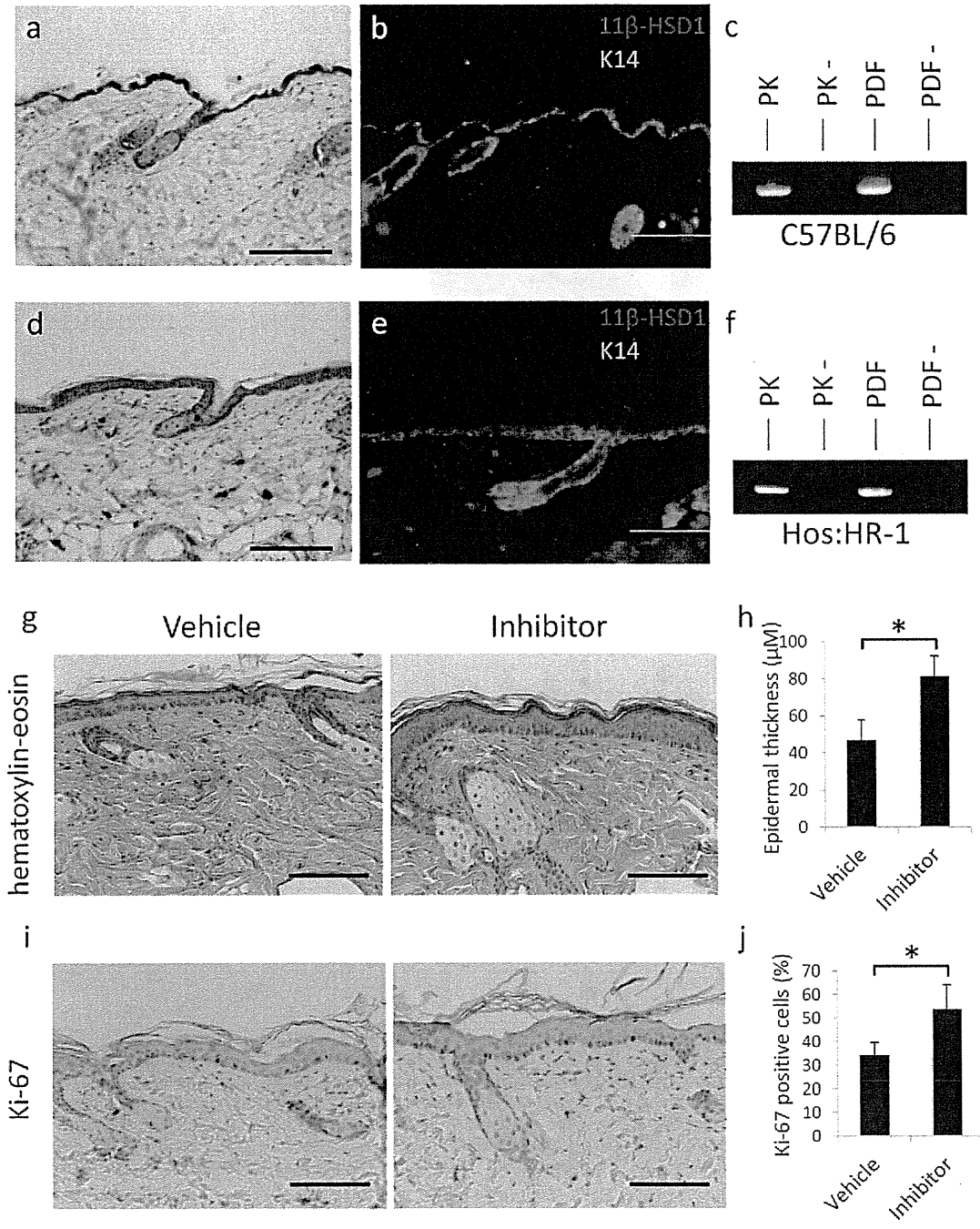

Figure 5. Selective inhibitor of 11β-HSD1 proliferates keratinocytes in murine skin. (a, d) Immunohistochemical staining of 11β-HSD1 (DAB staining) in C57BL/6 mouse (a) and Hos: HR-1 (hairless) mouse (d) skin tissue. Bar = 50 μM. (b, e) Immunofluorescent staining of 11β-HSD1 (red) and keratin 14 (green) in C57BL/6 mouse (b) and Hos: HR-1 mouse (e) skin tissue. Bar = 100 μM. (c, f) PCR detecting 11β-HSD1 in primary mouse keratinocytes and primary mouse dermal fibroblasts of C57BL/6 mouse (c) and Hos: HR-1 mouse (f). RT-: samples without reverse transcriptase (negative control). (g–j) Representative H&E staining (g) and Ki-67 staining (i) of 11β-HSD1 selective inhibitor or vehicle (1:1, acetone:olive oil) treated skin of Hos: HR-1 mice. Bar = 100 μm. (h) Epidermal thickness of vehicle and inhibitor treated mice. Intrafollicular epidermal thickness was calculated by averaging five locations in each section. Three sections from each mouse were evaluated. Bars show mean epidermal thickness ± SD of vehicle-treated mice (n = 5) and inhibitor-treated mice (n = 5; *$P<0.01$, Student's *t*-test). (j) The percentage of Ki-67 positive cells. Analyses were performed by counting the total number of basal cells and cells expressing nuclear Ki-67 stain. Three sections from each mouse were evaluated. Bars indicate mean ± SD of vehicle-treated mice (n = 5) and inhibitor-treated mice (n = 5; *$P<0.05$, Student's *t*-test).
doi:10.1371/journal.pone.0025039.g005

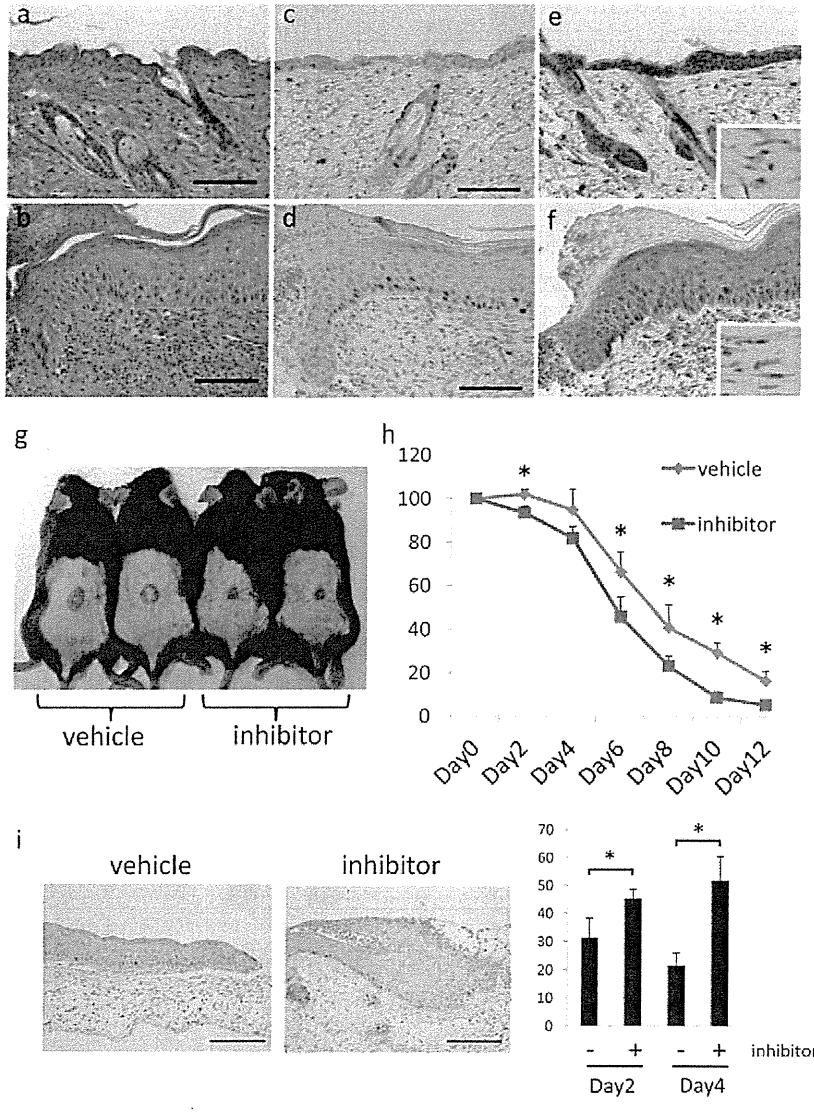

Figure 6. The role of 11β-HSD1 in wound healing of C57BL/6 mice. (a–f) H&E (a, b), Ki-67 (c, d), and 11β-HSD1 (e, f) staining of ulcer edge and non ulcer skin of the same section. Inserts: high magnification of the fibroblasts. Bar = 100 μm. (g) Macroscopic view of wound healing on day 10. A 15-mm wound was created on the back of 6-week-old male mice and wound closure was monitored with application of vehicle or 11β-HSD1 inhibitor every other day. (h) Reduction of wound area on days 2, 4, 6, 8, 10, and 12. The histograms indicate means and standard deviations for four mice in each group. An asterisk indicates a statistically significant difference (*$P<0.05$, Student's *t*-test). (i) Representative Ki-67 staining in day2 wound edge skin and the percentage of Ki-67 positive cells in day2 and day4 wound edge epidermis. Analyses were performed by counting the total number of basal cells and cells expressing nuclear Ki-67 stain. Bars indicate mean ± SD of vehicle-treated mice (n = 6) and inhibitor-treated mice (n = 6; *$P<0.05$, Student's *t*-test). Bar = 100 μm.
doi:10.1371/journal.pone.0025039.g006

11β-HSD1 inhibitor promotes wound healing in C57BL/6 mice

Taken together, these findings demonstrate that 11β-HSD1 regulates the proliferation of keratinocytes and fibroblasts. We therefore hypothesized that 11β-HSD1 inhibitor would promote wound healing. The keratinocytes at wound edges are hyperproliferative, thus the epidermis becomes thick in this region, with increased Ki-67 positive cells (Figure 6a–d). Interestingly, the intensity of 11β-HSD1 detected with immunohistochemical staining was lower in wound edge keratinocytes than in non wound keratinocytes in the same section (Figure 6e,f). The intensity of 11β-HSD1 did not differ between wound edge fibroblasts and non-wound fibroblasts (Figure 6e,f inserts). Because our data show that 11β-HSD1 negatively regulates the proliferation of keratinocytes, we considered that the decreased expression of 11β-HSD1 in wound edge keratinocytes might be promoting their proliferative state. To investigate whether selective 11β-HSD1 inhibitor could promote wound healing, we applied 10 μM 11β-HSD1 inhibitor every other day to wounds created on the dorsal skin of C57BL/6 mice. The wound areas were significantly smaller in the 11β-HSD1 inhibitor treated group than the vehicle treated group (Figure 6g,h). The number of Ki-67 positive cells was significantly higher on day2 and day4 wound edge epidermis in the 11β-HSD1 inhibitor treated group than the vehicle treated group (Figure 6i).

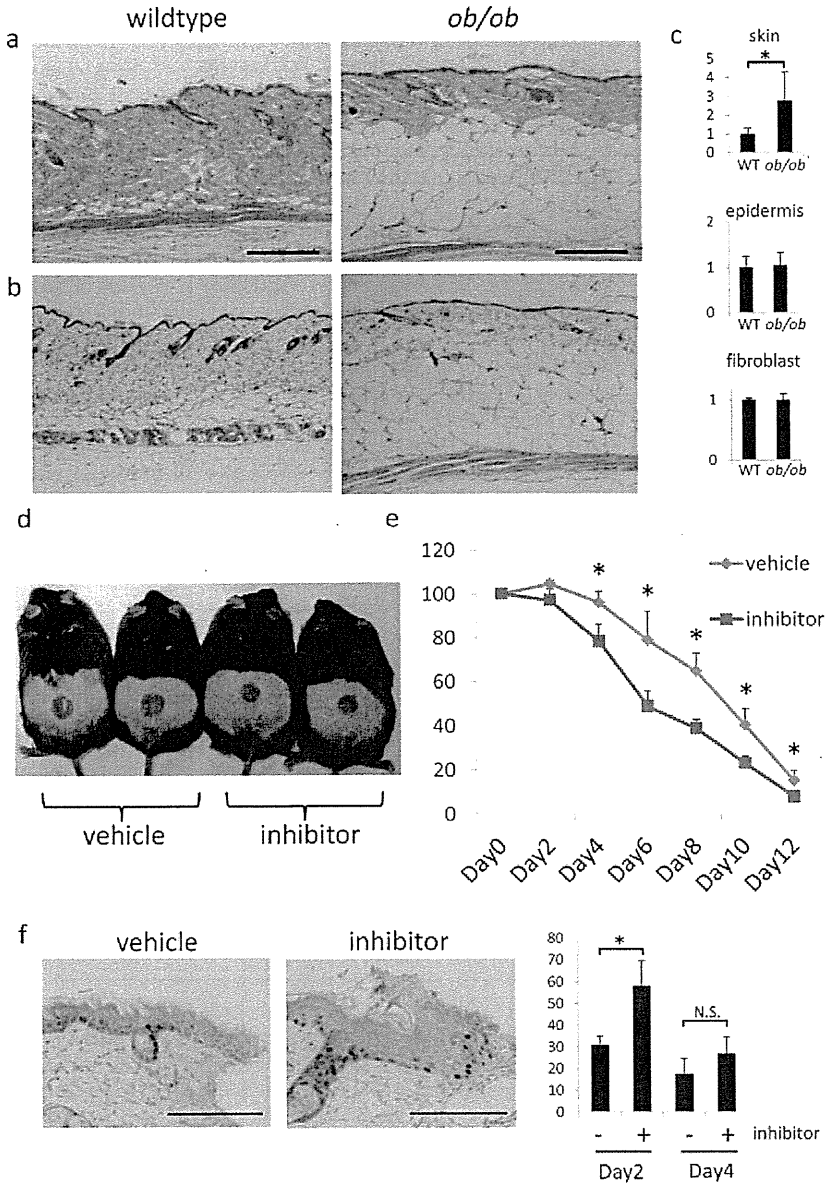

Figure 7. Selective 11β-HSD1 inhibitor enhance wound healing in *ob/ob* mice. (a,b) Representative H&E staining (a) and 11β-HSD1 staining (b) of 6-week-old male wildtype and *ob/ob* mice. Bar = 50 μm. (c) The relative expressions of 11β-HSD1 in epidermis, fibroblasts, and whole skin extract of wildtype and *ob/ob* mice assessed by rtPCR. GAPDH was used as an internal control ($P<0.05$, Student's *t*-test). (d) Macroscopic view of wound healing on day 8. A 15-mm wound was created on the back of 6-week-old male *ob/ob* mice and wound closure was monitored with application of vehicle or 11β-HSD1 inhibitor every other day. (e) Reduction of wound area on days 2, 4, 6, 8, 10, and 12. The histograms indicate means and standard deviations for four mice in each group. An asterisk indicates a statistically significant difference (*$P<0.05$, Student's *t*-test). (f) Representative Ki-67 staining in day4 wound edge skin and the percentage of Ki-67 positive cells in day2 and day4 wound edge epidermis. Analyses were performed by counting the total number of basal cells and cells expressing nuclear Ki-67 stain. Bars indicate mean ± SD of vehicle-treated mice (n = 3) and inhibitor-treated mice (n = 3; *$P<0.05$, Student's *t*-test). Bar = 100 μm.
doi:10.1371/journal.pone.0025039.g007

11β-HSD1 inhibitor promotes wound healing in *ob/ob* mice

We finally assessed wound healing in obese/obese (*ob/ob*) mice, the model of impaired wound healing. In *ob/ob* mice, the dermal layer was thinner, and the subcutaneous adipose layer was thicker, than in age-matched wildtype mice (Figure 7a). Interestingly, the expression of 11β-HSD1 was significantly higher in the skin extract of *ob/ob* mice, however, the expression did not differ in the epidermal extract and the fibroblast extract (Figure 7b,c). These data suggest that increased subcutaneous adipose tissue in *ob/ob* mice is responsible for increased expression of 11β-HSD1 in the skin extract. Notably, application of 10 μM 11β-HSD1 inhibitor every other day improved wound healing more in *ob/ob* mice than in C57BL/6 mice (Figure 7d and 7e). The number of Ki-67 positive cells was significantly higher on day2 wound edge epidermis in the 11β-HSD1 inhibitor treated group than the vehicle treated group (Figure 7f).

Discussion

The present study shows that 11β-HSD1 is a regulator of keratinocyte and fibroblast proliferation. We found that the expression of 11β-HSD1 is higher in the cytoplasm of supra-basal differentiating cells than in basal proliferating cells of the normal epidermis, and that the inhibition of 11β-HSD1 increases the proliferation of keratinocytes and fibroblasts. We also report that topical application of a selective 11β-HSD1 inhibitor promotes keratinocyte proliferation and wound healing.

Skin is one of the most chronically stress-loaded tissues because it faces the outside environment and is exposed to stressors including bacteria, ultraviolet radiation, and mechanical stimulation. Thus, it makes intuitive sense that skin expresses the functional cortisol activating enzyme 11β-HSD1. Specifically, our experiments using immunofluorescence staining revealed that 11β-HSD1 is expressed in the supra-basal area of the epidermis. This expression pattern of 11β-HSD1 is different from previous reports [17]. However, 11β-HSD1 expression being limited to the supra-basal epidermal area seems reasonable, considering that 11β-HSD1-mediated suppression of excessive proliferation in differentiated keratinocytes might contribute to maintain adequate epidermal thickness. In addition to its known anti-inflammatory properties, glucocorticoid (e.g., cortisol and corticosterone) is known to regulate the proliferation of keratinocytes and prolong epidermal turnover time [22,23,24,25]. Consistent with this, we have shown that selective inhibition of 11β-HSD1 promotes the proliferation of keratinocytes both *in vitro* and *in vivo*, suggesting that intracellular activators of cortisol would negatively regulate keratinocyte proliferation (Figure 3 and 5). Hence, we conclude that topical application of selective 11β-HSD1 inhibitor has the potential to be an effective treatment to stimulate the proliferation of keratinocytes. However, we observed that high doses of selective 11β-HSD1 inhibitor and siRNA knock down of 11β-HSD1 decreased the viability of keratinocytes. Thus, it is important to determine the optimal dosage to stimulate proliferation without unwanted toxic effects. Unexpectedly, the selective 11β-HSD1 inhibitor did not influence calcium-induced differentiation of keratinocytes. As calcium-induced differentiation *in vitro* differs from *in vivo* differentiation, further study may needed to determine if 11β-HSD1 plays a functional role in keratinocyte differentiation.

Glucocorticoids are known to increase in response to stress or medical therapy, and impair wound healing because they inhibit proliferation of cells and proinflammatory cytokine production [26,27]. In this study, we showed that 11β-HSD1 inhibitor significantly promotes cutaneous wound healing. We think the decrease in the expression of 11β-HSD1 in keratinocytes at wound edges might be a normal physiological mechanism that promotes the proliferation of keratinocytes during wound healing. Thus, the selective 11β-HSD1 inhibitor might promote wound healing because it supports this mechanism. The selective 11β-HSD1 inhibitor also promotes the proliferation of NHDFs *in vitro*, and the effect of the inhibitor on fibroblasts also might assist wound healing. The effect of inhibitor on endothelial cells and inflammatory cytokines, which also are important factors in wound healing, needs to be evaluated in the future.

It is intriguing that the inhibitor has a stronger effect on wound healing in *ob/ob* mice, a model of impaired wound healing. These mice exhibit severe diabetes and obesity syndromes, phenotypes mediated by the loss of the ob gene product: the 16 kDa cytokine leptin [28,29]. The expression of 11β-HSD1 is elevated in stromal vascular cells and mature adipocytes isolated from the adipose tissue of *ob/ob* mice [30]. Interestingly, the expression of 11β-HSD1 was also elevated in the skin extract of *ob/ob* mice (Figure 7c). The selective 11β-HSD1 inhibitor promoted wound healing in *ob/ob* mice, almost to the same level as the inhibitor treated group of C57BL/6 mice. Thus, we hypothesize that increased expression of 11β-HSD1 in *ob/ob* mouse skin might play an important role in delayed wound healing in *ob/ob* mice. The mouse skin extract is composed of epidermis, dermis, subcutaneous adipose tissue, and cutaneous muscular tissue. It was recently reported that subcutaneous adipose tissue is an important regulator of dermal fibroblast proliferation in high-fat diet induced obese mice [31]. It is possible that not only keratinocytes and fibroblasts, but also the subcutaneous adipose layer, which is markedly increased in *ob/ob* mice, could be a source of 11β-HSD1 in *ob/ob* mice as the expression of 11β-HSD1 did not differ in the epidermal extract and the fibroblast extract. We think that the 11β-HSD1 inhibitor might also act on the subcutaneous adipose tissue to accelerate wound healing in *ob/ob* mice, although further study is needed to test this theory.

Obesity is a global problem that affects 400 million adults worldwide [12,32]. Adipose tissue overexpression of 11β-HSD1 is observed in human obesity, and inhibition of 11β-HSD1 has been proposed to be of potential therapeutic benefit to patients with obesity and type 2 diabetes mellitus [33,34,35]. Our results suggest that in addition to systemic administration of 11β-HSD1 inhibitor, topical application of 11β-HSD1 inhibitor is potentially effective for the treatment of the chronic wounds of obese and diabetic patients.

In summary, the present study identifies a novel role for 11β-HSD1 in the promotions of keratinocyte and fibroblast proliferation. Targeting 11β-HSD1 could be a novel approach to treat chronic wounds, and skin diseases with aberrant proliferation.

Author Contributions

Conceived and designed the experiments: MT HM EM IK. Performed the experiments: MT KI A. Kimura A. Kato AI. Analyzed the data: MT A. Kimura. Contributed reagents/materials/analysis tools: MT. Wrote the paper: MT.

References

1. Sapolsky RM, Romero LM, Munck AU (2000) How do glucocorticoids influence stress responses? Integrating permissive, suppressive, stimulatory, and preparative actions. Endocr Rev 21: 55–89.
2. Zhou J, Cidlowski JA (2005) The human glucocorticoid receptor: one gene, multiple proteins and diverse responses. Steroids 70: 407–417.
3. Revollo JR, Cidlowski JA (2009) Mechanisms generating diversity in glucocorticoid receptor signaling. Ann N Y Acad Sci 1179: 167–178.
4. Adcock IM, Caramori G (2001) Cross-talk between pro-inflammatory transcription factors and glucocorticoids. Immunol Cell Biol 79: 376–384.
5. Stojadinovic O, Lee B, Vouthounis C, Vukelic S, Pastar I, et al. (2007) Novel genomic effects of glucocorticoids in epidermal keratinocytes: inhibition of apoptosis, interferon-gamma pathway, and wound healing along with promotion of terminal differentiation. J Biol Chem 282: 4021–4034.
6. Seckl JR, Walker BR (2001) Minireview: 11beta-hydroxysteroid dehydrogenase type 1- a tissue-specific amplifier of glucocorticoid action. Endocrinology 142: 1371–1376.
7. Sandeep TC, Walker BR (2001) Pathophysiology of modulation of local glucocorticoid levels by 11beta-hydroxysteroid dehydrogenases. Trends Endocrinol Metab 12: 446–453.
8. Ishii T, Masuzaki H, Tanaka T, Arai N, Yasue S, et al. (2007) Augmentation of 11beta-hydroxysteroid dehydrogenase type 1 in LPS-activated J774.1 macrophages–role of 11beta-HSD1 in pro-inflammatory properties in macrophages. FEBS Lett 581: 349–354.
9. Odermatt A, Atanasov AG, Balazs Z, Schweizer RA, Nashev LG, et al. (2006) Why is 11beta-hydroxysteroid dehydrogenase type 1 facing the endoplasmic reticulum lumen? Physiological relevance of the membrane topology of 11beta-HSD1. Mol Cell Endocrinol 248: 15–23.
10. Desbriere R, Vuaroqueaux V, Achard V, Boullu-Ciocca S, Labuhn M, et al. (2006) 11beta-hydroxysteroid dehydrogenase type 1 mRNA is increased in both visceral and subcutaneous adipose tissue of obese patients. Obesity (Silver Spring) 14: 794–798.
11. Mericq V, Medina P, Bouwman C, Johnson MC, Godoy J, et al. (2009) Expression and activity of 11beta-hydroxysteroid dehydrogenase type 1 enzyme

in subcutaneous and visceral adipose tissue of prepubertal children. Horm Res 71: 89–93.
12. Morton NM (2010) Obesity and corticosteroids: 11beta-hydroxysteroid type 1 as a cause and therapeutic target in metabolic disease. Mol Cell Endocrinol 316: 154–164.
13. Masuzaki H, Paterson J, Shinyama H, Morton NM, Mullins JJ, et al. (2001) A transgenic model of visceral obesity and the metabolic syndrome. Science 294: 2166–2170.
14. Masuzaki H, Yamamoto H, Kenyon CJ, Elmquist JK, Morton NM, et al. (2003) Transgenic amplification of glucocorticoid action in adipose tissue causes high blood pressure in mice. J Clin Invest 112: 83–90.
15. Tiganescu A, Walker EA, Hardy RS, Mayes AE, Stewart PM (2011) Localization, Age- and Site-Dependent Expression, and Regulation of 11beta-Hydroxysteroid Dehydrogenase Type 1 in Skin. J Invest Dermatol.
16. Hennebert O, Chalbot S, Alran S, Morfin R (2007) Dehydroepiandrosterone 7alpha-hydroxylation in human tissues: possible interference with type 1 11beta-hydroxysteroid dehydrogenase-mediated processes. J Steroid Biochem Mol Biol 104: 326–333.
17. Cirillo N, Prime SS (2011) Keratinocytes synthesize and activate cortisol: first characterisation of a novel epidermal glucocorticoid system. J Cell Biochem;in press.
18. Terao M, Murota H, Kitaba S, Katayama I (2010) Tumor necrosis factor-alpha processing inhibitor-1 inhibits skin fibrosis in a bleomycin-induced murine model of scleroderma. Exp Dermatol 19: 38–43.
19. Hermanowski-Vosatka A, Balkovec JM, Cheng K, Chen HY, Hernandez M, et al. (2005) 11beta-HSD1 inhibition ameliorates metabolic syndrome and prevents progression of atherosclerosis in mice. J Exp Med 202: 517–527.
20. Micallef L, Belaubre F, Pinon A, Jayat-Vignoles C, Delage C, et al. (2009) Effects of extracellular calcium on the growth-differentiation switch in immortalized keratinocyte HaCaT cells compared with normal human keratinocytes. Exp Dermatol 18: 143–151.
21. Bikle DD, Oda Y, Xie Z (2004) Calcium and 1,25(OH)2D: interacting drivers of epidermal differentiation. J Steroid Biochem Mol Biol 89–90: 355–360.
22. Choi EH, Demerjian M, Crumrine D, Brown BE, Mauro T, et al. (2006) Glucocorticoid blockade reverses psychological stress-induced abnormalities in epidermal structure and function. Am J Physiol Regul Integr Comp Physiol 291: R1657–1662.
23. Sheu HM, Tai CL, Kuo KW, Yu HS, Chai CY (1991) Modulation of epidermal terminal differentiation in patients after long-term topical corticosteroids. J Dermatol 18: 454–464.
24. Zoller NN, Kippenberger S, Thaci D, Mewes K, Spiegel M, et al. (2008) Evaluation of beneficial and adverse effects of glucocorticoids on a newly developed full-thickness skin model. Toxicol In Vitro 22: 747–759.
25. Demerjian M, Choi EH, Man MQ, Chang S, Elias PM, et al. (2009) Activators of PPARs and LXR decrease the adverse effects of exogenous glucocorticoids on the epidermis. Exp Dermatol 18: 643–649.
26. Hubner G, Brauchle M, Smola H, Madlener M, Fassler R, et al. (1996) Differential regulation of pro-inflammatory cytokines during wound healing in normal and glucocorticoid-treated mice. Cytokine 8: 548–556.
27. Christian LM, Graham JE, Padgett DA, Glaser R, Kiecolt-Glaser JK (2006) Stress and wound healing. Neuroimmunomodulation 13: 337–346.
28. Coleman DL (1978) Obese and diabetes: two mutant genes causing diabetes-obesity syndromes in mice. Diabetologia 14: 141–148.
29. Zhang Y, Proenca R, Maffei M, Barone M, Leopold L, et al. (1994) Positional cloning of the mouse obese gene and its human homologue. Nature 372: 425–432.
30. Ishii-Yonemoto T, Masuzaki H, Yasue S, Okada S, Kozuka C, et al. (2010) Glucocorticoid reamplification within cells intensifies NF-kappaB and MAPK signaling and reinforces inflammation in activated preadipocytes. Am J Physiol Endocrinol Metab 298: E930–940.
31. Ezure T, Amano S (2010) Increased subcutaneous adipose tissue impairs dermal function in diet-induced obese mice. Exp Dermatol 19: 878–882.
32. Rigby NJ, Kumanyika S, James WP (2004) Confronting the epidemic: the need for global solutions. J Public Health Policy 25: 418–434.
33. Bujalska IJ, Gathercole LL, Tomlinson JW, Darimont C, Ermolieff J, et al. (2008) A novel selective 11beta-hydroxysteroid dehydrogenase type 1 inhibitor prevents human adipogenesis. J Endocrinol 197: 297–307.
34. Hollis G, Huber R (2011) 11beta-Hydroxysteroid dehydrogenase type 1 inhibition in type 2 diabetes mellitus. Diabetes Obes Metab 13: 1–6.
35. Hale C, Wang M (2008) Development of 11beta-HSD1 inhibitors for the treatment of type 2 diabetes. Mini Rev Med Chem 8: 702–710.

JBC Papers in Press. Published on June 22, 2011 as Manuscript M111.220376
The latest version is at http://www.jbc.org/cgi/doi/10.1074/jbc.M111.220376

ENHANCED EPITHELIAL-MESENCHYMAL TRANSITION-LIKE PHENOTYPE IN *N*-ACETYLGLUCOSAMINYLTRANSFERASE V TRANSGENIC MOUSE SKIN PROMOTES WOUND HEALING

Mika Terao[1,2]*, Akiko Ishikawa[1]*, Susumu Nakahara[3], Akihiro Kimura[1], Arisa Kato[1], Kenta Moriwaki[1], Yoshihiro Kamada[1], Hiroyuki Murota[2], Naoyuki Taniguchi[3], Ichiro Katayama[2], Eiji Miyoshi[1,3]

From Department of Molecular Biochemistry and Clinical Investigation[1], Department of Dermatology[2], Department of Biochemistry[3], Osaka University Graduate School of Medicine.

*These authors equally contribute to this work.

Running head: EMT-like phenotype in GnT-V Tg mice

Address correspondence to: Department of Molecular Biochemistry and Clinical Investigation, 1-7, Yamada-oka, Suita 565-0871, Japan. Fax: +81-6-6879-2590; E-mail: emiyoshi@sahs.med.osaka-u.ac.jp

***N*-Acetylglucosaminyltransferase-V (GnT-V) catalyzes the β1,6 branching of *N*-acetylglucosamine on *N*-glycans. GnT-V expression is elevated during malignant transformation in various types of cancer; however, the mechanism by which GnT-V promotes cancer progression is unclear. To characterize the biological significance of GnT-V, we established GnT-V transgenic (Tg) mice, in which GnT-V is regulated by a β-actin promoter. No spontaneous cancer was detected in any organs of the GnT-V Tg mice. However, GnT-V expression was upregulated in GnT-V Tg mouse skin, and cultured keratinocytes derived from these mice showed enhanced migration, which was associated with changes in E-cadherin localization, and epithelial-mesenchymal transition (EMT). Further, EMT–associated factors snail, twist, and, N-cadherin were upregulated, and cutaneous wound healing was accelerated *in vivo*. We further investigated the detailed mechanisms of EMT by assessing epidermal growth factor (EGF) signaling and found upregulated EGF receptor signaling in GnT-V Tg mouse keratinocytes. These findings indicate that GnT-V overexpression promotes EMT and keratinocyte migration in part through enhanced EGF receptor signaling.**

Oligosaccharide structure changes are detected following birth, differentiation, and carcinogenesis (1), and these changes are regulated by glycosyltransferases. In particular, *N*- acetylglucosaminyltransferase V (GnT-V) plays an important role in carcinogenesis and tumor metastasis (2). To characterize the detailed molecular mechanisms underlying GnT-V—related tumor metastasis, we and other groups succeeded in purifying and cloning GnT-V (3-5). In addition, we developed a sugar remodeling system of cancer cells and demonstrated the biological function of GnT-V in tumor metastasis through biochemical analysis of its target glycoproteins (6). Dennis et al. reported that mammary tumor growth and metastases induced by the polyomavirus middle T oncogene was considerably less in GnT-V deficient mice than in littermate control mice. (7). Cancer cells established from GnT-V–deficient mice showed lower cell growth and intracellular signaling than control mice because of aberrant glycosylation of growth factor receptors (8). Dennis et al. also reported that sugar metabolism is critical to control the formation of β1,6 *N*-acetylglucosamine (GlcNAc), a product of GnT-V (9). In contrast, GnT-V is involved in negative regulation of T cell activation, leading to suppress autoimmunity reaction (10). Recently, Mkhikian *et al.* reported that genetic changes in glycosylation status for suppressing *N*-glycan branching are concerned with the incidence of Multiple Sclerosis (11). Our groups have studied biological functions of adhesion molecules such as cadherin and integrins in terms of N-glycan branching mediated by GnT-V and have found that GnT-V inhibits cell-cell/cell-matrix adhesion and promotes migration of cancer cells (12).

Although GnT-V is known to be upregulated in the early phase of carcinogenesis in many cancers (13), it is unclear whether